Applied Energy

Thermal Energy Efficiency Optimization for Paint Curing Process: Three-dimensional Numerical Modelling of Industrial Automotive Oven

--Manuscript Draft--

Manuscript Number:	APEN-D-23-03959
Article Type:	Research Paper
Keywords:	Paint ovens; Conjugate heat transfer (CHT); Thermal energy efficiency; Geometrical optimization; Automotive industry; Large-eddy simulation (LES)
Corresponding Author:	Mohammad-Reza Pendar Universidade da Beira Interior
First Author:	Mohammad-Reza Pendar, Phd
Order of Authors:	Mohammad-Reza Pendar, Phd
	José Carlos Páscoa, Phd
	Rui Lima
Abstract:	The impetus of the present work is to propose a comprehensive methodology for numerical evaluation of the drying/curing process, as one of the most complex energy-consuming stages in the paint shop plant, to guarantee a decrease the energy costs without sacrificing final paint film quality and manufacturability. An optimization-based redesigning and effective parametric modification of conjugate heat transfer (CHT) in an automotive oven are implemented. The vehicle assembly's complicated geometry, multi-zoned oven with a high level of complexity, transient process nature, flows varying scales, and tightly coupled conjugate heat transfer among solid and fluid are considered that clarify the complexity of the current modeling. A developed efficient conjugate heat transfer algorithm under the OpenFOAM package framework is employed for modeling the heat-up turbulence flow with detailed recirculation pattern, severe stress and strain rate inside the oven with the accompaniment of the Large Eddy Simulation (LES) turbulence model. The code is validated using heat sink cases, which comprise similar flow physics nature compared to flow in the oven. A good agreement is obtained compared to experimental results, considering the average Nusselt number and heat transfer coefficient parameters. Applying modification for the intake supply heated airflow rate/direction and geometrical optimization leads to optimum recirculation growth in the measured mean temperature along with the curing oven and the car body surface, saving a significant amount of energy. All the fluid dynamic characteristics, e.g., mean velocity and temperature distribution, air circulation detected structure/nature, turbulent kinetic energy, streamwise velocity fluctuation, and thermal stresses across all multi-zoned oven lengths and over the vehicle body during the curing of the paint layers, are reported. The optimized panels and nozzles arrangement/flow rate that resulted in an increment in hot air volume circulation, for the region need attention, especially the oven's lower half, is described.
Suggested Reviewers:	Ehsan Roohi, Phd Professor, Xi'an Jiaotong University e.roohi@xjtu.edu.cn He has extensive experience in numerical CFD simulation and can be named one of the best in the field, like the current paper.
	Seyed Mahmood Mousavi, Phd Post-doctoral Researcher, Texas State University sm.mousavi@shirazu.ac.ir He has lots of extensive experience in numerical CFD simulation and can be named as one of the international leaders in the field of the current paper.
	Carlos Xisto, Phd Professor, Chalmers University of Technology carlos.xisto@chalmers.se He has investigated different problems same as the field of our presented paper.
	Esmaeil Esmaeilifar, Phd

	Phd, Gyeongsang National University e.esmaeilifar@gmail.com He has lots of extensive experience in numerical CFD simulation and can be named as one of the best in the field of the current paper.
	Frederico Rodrigues, Phd Professor, University of Beira Interior fredmfr@hotmail.com He has investigated different problems exactly same as the field of our presented paper.

UNIVERSIDADE DA BEIRA INTERIOR
Faculdade de Engenharia

Cover Letter

2nd May 2023

To the Editor,

Journals of Applied Energy

Dear Editor,

I am writing to submit the manuscript "**Optimization of Thermal Energy Efficiency for Paint Curing Process: 3D Numerical Modelling of Automotive Industrial Oven**". In this manuscript, we proposed a comprehensive methodology for numerical evaluation of the drying/curing process, as one of the most complex energy-consuming stages in the paint shop plant, to guarantee a decrease the energy costs without sacrificing final paint film quality and manufacturability. An optimization-based redesigning and effective parametric modification of conjugate heat transfer (CHT) in an automotive multi-zoned oven are implemented. This manuscript describes the original work and is not under consideration by any other journal. All authors approved the manuscript and their submission.

Thank you for receiving our manuscript and considering it for review. We appreciate your time and looking forward to your response.

Best Regards,

Mohammad-Reza Pendar

Calçada Fonte do Lameiro,
6201-001 Covilhã, PORTUGAL

Thermal Energy Efficiency Optimization for Paint Curing Process: Three-dimensional Numerical Modelling of Industrial Automotive Oven

Mohammad-Reza Pendar[a,1], José Carlos Páscoa[a], Rui Lima[b]

[a]University of Beira Interior, Department of Electromechanical Engineering, C-MAST (Center for Mechanical and Aerospace Sciences and Technologies)

[a]FCT (Portuguese Foundation for Science and Technology) Research Unit Nº 151, Covilhã, Portugal

[b]CCEnergia Lda Rio Maior, Portugal

Abstract

The impetus of the present work is to propose a comprehensive methodology for numerical evaluation of the drying/curing process, as one of the most complex energy-consuming stages in the paint shop plant, to guarantee a decrease the energy costs without sacrificing final paint film quality and manufacturability. An optimization-based redesigning and effective parametric modification of conjugate heat transfer (CHT) in an automotive oven are implemented. The vehicle assembly's complicated geometry, multi-zoned oven with a high level of complexity, transient process nature, flows varying scales, and tightly coupled conjugate heat transfer among solid and fluid are considered that clarify the complexity of the current modeling. A developed efficient conjugate heat transfer algorithm under the OpenFOAM package framework is employed for modeling the heat-up turbulence flow with detailed recirculation pattern, severe stress and strain rate inside the oven with the accompaniment of the Large Eddy Simulation (LES) turbulence model. The code is validated using heat sink cases, which comprise similar flow physics nature compared to flow in the oven. A good agreement is obtained compared to experimental results, considering the average Nusselt number and heat transfer coefficient parameters. Applying modification for the intake supply heated airflow rate/direction and geometrical optimization leads to optimum recirculation growth in the measured mean temperature along with the curing oven and the car body surface, saving a significant amount of energy. All the fluid dynamic characteristics, e.g., mean velocity and temperature distribution, air circulation detected structure/nature, turbulent kinetic energy, streamwise velocity fluctuation, and thermal stresses across all multi-zoned oven lengths and over the vehicle body during the curing of the paint layers, are reported. The optimized panels and nozzles arrangement/flow rate that resulted in an increment in hot air volume circulation, for the region need attention, especially the oven's lower half, is described.

Keywords: Paint ovens; Conjugate heat transfer (CHT); Thermal energy efficiency; Drying/curing process; Geometrical optimization; Automotive industry; CFD; Large-eddy simulation (LES)

[1] Corresponding author. Tel.:+351925467631; fax:+351275329972. E-mail addresses: m.reza.pendar@ubi.pt.

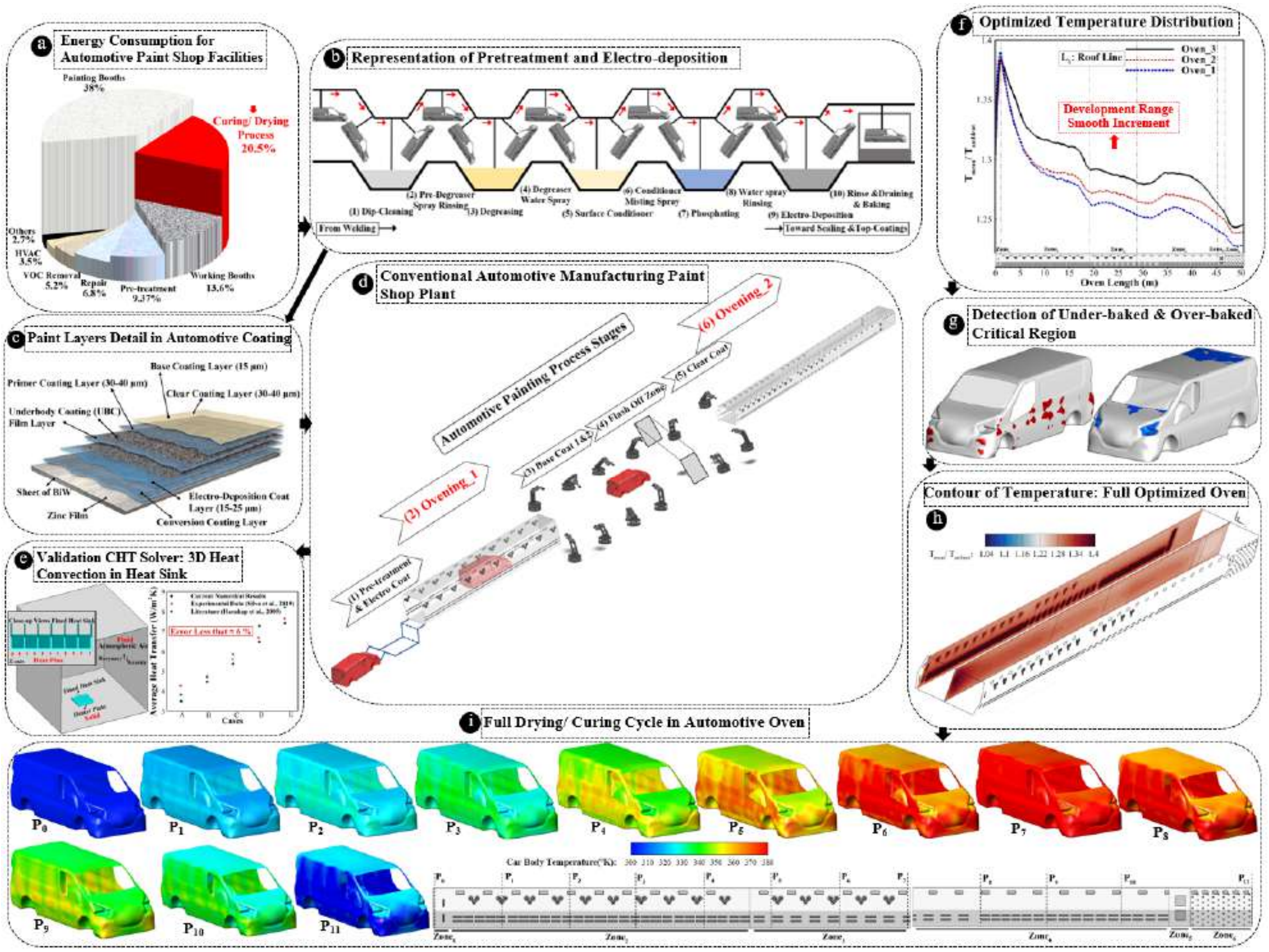

Graphical Abstract

1. Introduction and Motivation

The “paint curing” process, which defies as a drying of wet or powdered liquid paint to a hard film, is the most critical step in determination of the final paint film quality and is a significant energy consumer in the paint shop industries. During the last two decades, by growing the vehicles’ mass production rate, higher demand for faster curing time along with satisfying high film quality in terms of visual appearance, corrosion, and durability was taken into consideration. The main implemented strategies were retrofitting, optimizing, or redesigning the previous ovens with a particular view on increasing their energy efficiency. In the automotive industry, paint curing ovens consume more than 20% of the paint shop’s total energy (Rao and Gopinath, 2013). More than 25% of the energy is wasted due to suboptimal design, particularly at the startup and setback curing duration. The main sources of energy-wasting during drying/curing in automotive paint shops are ovens, furnaces, dryers, and boilers, which need special attention (Giampieri et al., 2020). According to Niamsuwan et al. (2015), wall and stored heat loss, waste gas loss, and entrance radiation loss are the most common sorts of heat loss in the auto oven. This proves the importance of further and precise numerical assessment of the thermo-fluid-solid coupling scenario and turbulence flow physics inside the automotive curing ovens for thermal energy management, savings and recovery, with high paint film quality (Despotovic and Babic, 2018). The present high-fidelity numerical investigation of thermo-fluid-solid coupling turbulence treatment is tried to guarantee optimization and control of the above-mentioned losses and develop oven efficiency.

The most significant paint film curing mechanisms include solvent loss, chemical reaction, oxidation, melting, and resolidifying (Ajah and Ejiogu, 2019). The heat transfer rate, curing time and temperature distribution are three determining references for energy consumption optimization during the drying/curing stage, avoiding under-curing or over-curing phenomenon, offered in the paint cure window (PCW) (Ashrafizadeh et al., 2009; Nazif, 2019; Ajah and Ejiogu, 2019). To obtain a corrosion protective film layer of paint, controlling two challenging parameters of the curing temperature (to prevent exposing crude or over-cures ranges) and the amount of consumed energy in the oven is significant (Ajah and Ejiogu, 2019). The formed paint film quality strongly depends on the conveyor pace and the homogeneity of the temperature distribution, which are controlled by empirical approaches (Cavalcante et al., 2020). Fig. 1a exhibits a schematic of a typical PCW, which defines the temperature ranges for the specified heating time with tolerances to reach desired drying/curing quality, as well as maximum (T_{max}) and minimum (T_{min}) temperatures as limitations (Prendi et al., 2015; Xiao et al., 2006). If the paint film reaches above the T_{max} or under the T_{min}, regardless of curing time, it can be considered an "overbaked/burned-out" or "underbaked" film, respectively. Similarly, the transformed temperature (TT) designed curve, which its computation is a standard method to check the cured paint film quality, is shown in Fig. 1a (Pendar and Páscoa, 2022a). The paint curing process is regarded as appropriate when the TT curve enters and exits from the AB and BC lines, respectively. If the cure time becomes lower or excessive for the TT curve to cross the AB and CD lines, the paint film will be "overbaked" or "underbaked", respectively. The curves that are obtained by measuring the temperature history at the vehicle body critical points are called an ideal curing procedure, as shown in Fig. 1b for the primer coat application (Wonnemann, 2008).

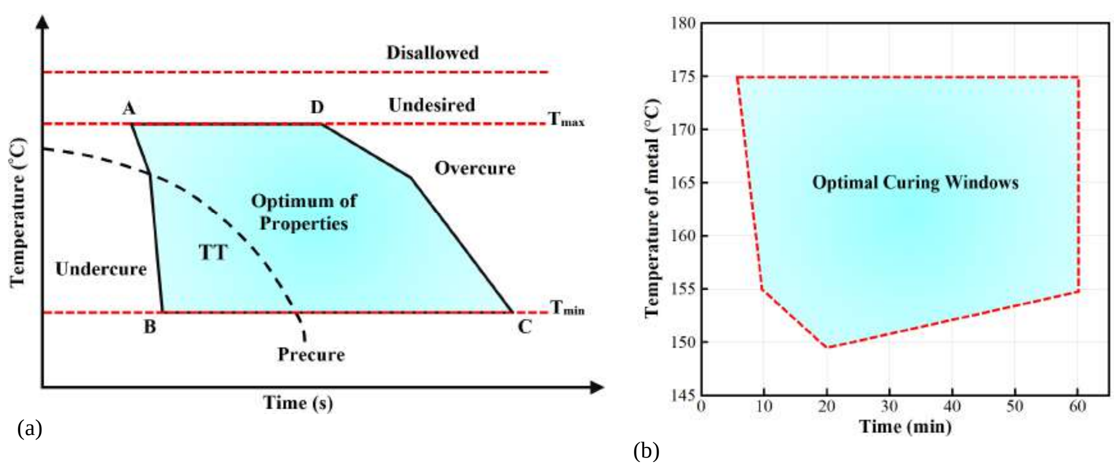

Fig. 1. Schematic representation of (a) the paint cure window (PCW) operational criteria for an automotive oven, and (b) optimal curing operational conditions for the primer coat layer.

Automotive mass production rate growth involves the employment of faster curing protectors with optimal lengths to supply mild hot flow without gradient (Streitberger and Dossel, 2008). Due to the high costs of the computational fluid dynamics (CFD) modeling, complicated geometry of the oven and car, complex physical processes, diverse scales of transient flows, and execution of a moving mesh with many bodies in the long-length oven, automotive continuous ovens are rarely addressed numerically in the literature (Pendar et al., 2022a; 2022b). The prominent publications that investigated the drying/curing process are presented in the following. Most of them implemented simplified models of the paint-curing oven when they applied various numerical methodologies.

The transient behavior of multi-stream heat exchangers, which occurs in numerous applications, such as the curing oven of automotive, aerospace, and chemical industries, are modeled with many simplification assumptions in several references Shrivastava and Ameel (2004), Bielski and Malinowski (2005), Mishra et al. (2008), Rao (2013). Xiao et al. (2006) introduced an innovative, proactive quality control (QC) methodology for curing of vehicle's topcoat, which evaluated film curing quality using dynamic process-product approaches. Rao and Teeparthi (2011) applied and developed an innovative semi-computational model and dual solver to model the oven's heat-up stage with the specific arrangement of nozzles. They examined the steady-state temperature map on the Body in White (BiW) surface during the transient heat transfer. After that, Rao (2013) reformed the equations for implementing the complex flow pattern in automobile paint ovens that are distributed in all directions in the same manner as they performed in the heat exchangers. Wu et al. (2013) suggested a methodology based on approximating the transient convection field with intermittent steady-state solutions to create an effective modeling strategy. They demonstrated how their approach permits acceptable outcomes compared to experimental data in less computational time and lowers dependence on the grid quality. Mulemane et al. (2015) suggest reduced-order models by manipulating associated differential equations for oven thermal modeling, including lump capacities. Despotovic and Babic (2018) proposed a simple mathematical approach for modeling energy flows in the curing oven to examine which variables, e.g., heated airflow or body temperature, are more prevalent throughout the vehicle paint curing operation during its redesigning to reach the desired temperature. Vasudevan (2018) focused on the paint curing procedure in the convective ovens and reported the transient residual weight and temperature values achieved at the top of the paint layer and the bottom of the metal substrate during the paint curing process. Nazif (2019) used a low-fidelity turbulence model, realizable k-ε, to model the heat-up stage of the car wax oven and compared the results with the experimental data. They improved the energy efficiency of the oven (air temperature ranges) up to 25 % by optimizing the design and airflow circulation. Giampieri et al. (2020) reported a detailed investigation into the management of energy and thermal efficiency to decrease the energy consumption in the paint curing procedure during car manufacturing.

Ye et al. (2009), Domnick et al. (2011) and Yu (2013) used the developed FLUENT commercial software to model the drying/curing process of the water-based paint films, mass treatment and ternary mixture heat transfer on the goal surface in the automotive oven. By analyzing the obtained local temperature gradients on the body at the oven's heating and cooling stages, they found helpful information for developing the predicted paint film quality. Zelder and Steinbeck-Behrens (2009) operated the virtual paint simulator (VPS) commercial software to examine the paint viscous behavior and temperature plot along with the automotive oven and the BiW surface during the curing operation. From another point of view, Albiez et al. (2011) employed Abaqus software to model the thermo-mechanical behavior of the coated and cured aluminum alloy surface. They measured the temperature field on the chassis surface at various instants and examined how the transient temperature is related to multiple mechanical characteristics of it. Johnson et al. (2022) modeled the conjugate heat transfer coupling at the interface of a simplified fluid-solid case, using industrial path solutions (IPS) software, to optimize the curing mechanism of the truck cab at the Scania plant. Pendar and Páscoa (2022b) performed a numerical analysis of the conjugate heat transport process in an automotive paint oven using a modified algorithm in combination with the LES turbulence model. They found considerable energy efficiency increases by implementing low-cost optimization of the input hot flow rate and revamping the oven's heat-up, holding, and cooling stages. The info above on curing process modeling in terms of software framework clarifies that the developed code of the open-source OpenFOAM software is employed for the first time in the present study.

Seubert and Nichols (2010) experimentally examined the automotive epoxy clearcoats curing. Brinckmann et al. (2011) implemented experiments on an automotive water-based paint-drying process on a laboratory scale and validated the obtained data in software. Later, Chen et al. (2014) experimentally investigated the car paint curing process utilizing the moving-window 2D correlation spectroscopy method that integrated with the principal component analysis. But given the numerous challenges associated with conducting experiments in an oven, they considered a curing method without temperature influence and allowed the paint to dry. Choi et al. (2016) performed experiments for combined near-infrared ranges in a convective curing oven to optimize the system's operation. Agha and Abu-Farha (2021) proposed a new experimental approach to capture the induced curing effects in adhesively bonded joints. Moreover, Sukhodolya et al. (2021) concerned the paint curing mechanisms by examining the thermo-mechanical curves. The lack of experimental works analysis on the automotive paint curing oven in literature due to its high expenses, unpredictability, and time-consuming are apparent.

A short introduction to the practical conventional curing process (Fig. 2a) in an automotive paint shop, based on reference Kameš (2014), is as follows. The car's body passes through the curing/drying oven, and the cataphoresis paint on the surface with a thickness of ≈10 to 20 μm exposed to heat with an average temperature of ≈170°C for around 30 minutes. Subsequently, after implementing the clear coat and base coat layers spraying process, the body paint film layers are baked in a curing oven with an average temperature of ≈140°C and ≈ 80°C for roughly 20 minutes and 5 minutes, respectively. Various new innovative painting and curing strategies, which are implemented to reduce the process complexity and energy-saving in the automotive paint shop, are also presented in Fig. 2. One of the best methods for minimizing paint shop energy use is to eliminate the primer coating booth and curing oven (Fig. 2b). The 2-wet approach as a successful strategy can coat on a wet paint surface, eliminating the curing/drying process between paint film layers coating, considerably reducing energy consumption and VOC and CO_2 emissions (Fig. 2c). Additionally, in recent years a novel method based on 3-wet painting, using only one curing process after three layers of deposition, was introduced by Ford and Mazda, which resulted in the best environmental performance. (Fig. 2d) (Pendar et al., 2022a). The high gradient of turbulent flow inside the paint drying/curing oven, because of various inlet airflow rates from nozzles and panels in diverse directions, makes selecting an appropriate turbulence model a critical issue. The LES turbulence model can better capture the internal flow and vortical structures (Pendar and Páscoa, 2022b; 2022c).

The paper is organized as follows: Sec. 2 illustrates the mathematical model and the numerical implementation utilized for simulations; Sec. 3 represents the oven and supplies details on the simulation settings; Sec. 4 is focused on the analysis of the fluid-thermal field inside the curing oven; in Sec. 5, concluding remarks are given.

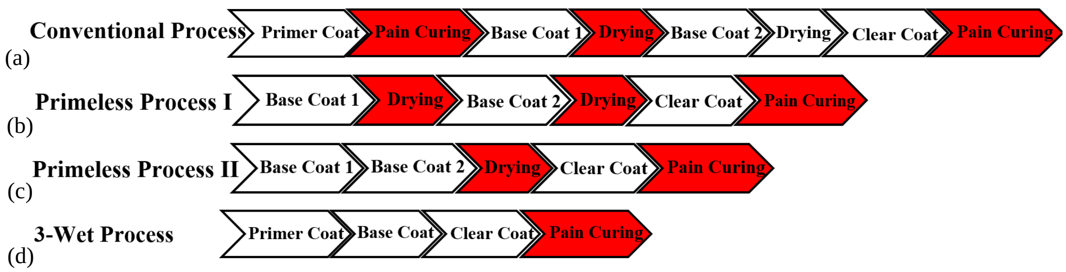

Fig. 2. Various available methods of the coating/curing processes representation in the automotive paint shop of the manufacturing plant.

2. Simulation Methodology

2. 1. Mathematical model

The thermal interaction study between the solid region and continuous fluid phase involves three primary actors: the fluid (heated air inside the oven) with its inner dynamics' circuits, heat diffusion in the solid (car chassis, conveyor, panel, and nozzle's base walls) and heat transfer at the interface. This work simulates these phenomena through the following appropriate set of models.

Fluid Region

The Favre average compressible Navier-Stokes (NS) equations, applying the Large Eddy Simulation (LES) filtering technique are presented. The LES turbulence model is conformed to computing the larger and energy-containing eddies and modeling the smaller sub-grid during the computational grid. The LES turbulent model provides this capability to govern the high strain and stress rate of the complicated flow inside the oven. In using the LES, all variables, i.e., f, are split into sub-grid scale (SGS) (f') and grid scale (GS) ($\overline{f}$) components, $f = f' + \overline{f}$. In the GS component $\overline{f} = G * f$, the $G = G(X, \Delta)$ is the filter function and $\Delta = \Delta(X)$ is the filter width (Ghosal, 1996). We employed the top-hat filter (De Villiers, 2006) as follows under the OpenFOAM source code:

$$G(x,\Delta) = \begin{cases} 1/\Delta: & if\ (x \le \Delta/2) \\ 0: & otherwise \end{cases}, \tag{1}$$

The grid spacing is used as the basis for setting the filter width Δ (De Villiers, 2006). The top-hat (box) filter is an implicit filter, which is dependent on the grid spacing and, in turn controls whether the smallest scales are retained. In this work, we modeled all the scales below the filter width Δ ,and employed "smooth" delta, as described in detail in reference Roohi et al. (2016). The gradient of the smoothed distribution is fixed by an adjustable coefficient of $C_{\Delta S}$ as follows:

$$\Delta = \max(\Delta_P, \Delta_N / C_{\Delta S}) \tag{2}$$

where P and N are mentioning the present cell and neighbor cell, respectively.

The equation for the conservation of mass is given as follows:

$$\frac{\partial \overline{\rho}}{\partial t} + \frac{\partial(\overline{\rho}\tilde{u}_i)}{\partial x_j} = 0, \tag{3}$$

here, $\tilde{u}_i$, ρ and t are the fluid velocity vector, density and time, respectively. The momentum conservation is as follow:

$$\frac{\partial \bar{\rho}\tilde{u}_i}{\partial t}+\frac{\partial}{\partial x_i}(\bar{\rho}\tilde{u}_i\tilde{u}_j)=-\frac{\partial \bar{p}}{\partial x_i}+\frac{\partial}{\partial x_j}\tilde{\sigma}_{ij}-\frac{\partial \tau_{ij}}{\partial x_j}, \tag{4}$$

in which $\tilde{\sigma}_{ij}$ and p are the viscous stress tensor and pressure, respectively. $\tilde{\sigma}_{ij}$ is defined as:

$$\tilde{\sigma}_{ij}=\bar{\mu}(\frac{\partial \tilde{u}_i}{\partial x_j}+\frac{\partial \tilde{u}_j}{\partial x_i}-\frac{2}{3}\delta_{ij}\frac{\partial \tilde{u}_k}{\partial x_k}), \tag{5}$$

where $\bar{\mu}$ and δ_{ij} denote the kinematic viscosity and Kronecker delta function, respectively. The unresolved transport part, the SGS, τ_{ij}, is defined as mentioned in reference Bensow and Fureby (2007):

$$\tau_{ij}\approx\rho(\widetilde{u_i u_j}-\tilde{u}_i\tilde{u}_j)\ . \tag{6}$$

The Eq. 6 needs to be modeled using one of the popular sub-grid approaches. Here the eddy-viscosity model is employed as follows:

$$\tau_{ij}=\frac{2}{3}\bar{\rho}kI-2\mu_k\overline{S_{ij}}\ , \tag{7}$$

$$\overline{S_{ij}}=\frac{1}{2}(\frac{\partial \overline{u_i}}{\partial x_j}+\frac{\partial \overline{u_j}}{\partial x_i})\ . \tag{8}$$

where $\overline{S_{ij}}$ is the resolved scale's strain rate tensor, and a "Local Eddy-Viscosity" method solves the sub-grid scale turbulent viscosity, μ_k. Applying the "one equation eddy viscosity model" (OEEVM) sub-grid scale (SGS) approach preserves an LES turbulence model (Pendar and Roohi, 2018; Pendar and Páscoa, 2022c). In the present analysis, the OEEVM sub-grid scale model is utilized. To calculate the turbulence kinetic energy *k*, the OEEVM approach solves the following equations:

$$\partial(\bar{\rho}k)+\nabla.(\bar{\rho}k\tilde{u})=-\tau_{ij}.\overline{S_{ij}}+\nabla.(\mu_k\nabla k)+\bar{\rho}\varepsilon\ , \tag{9}$$

$$\varepsilon=c_\varepsilon k^{3/2}/\Delta\ , \tag{10}$$

$$\mu_k=c_k\bar{\rho}\Delta\sqrt{k}\ . \tag{11}$$

In this model Δ is the filter width, c_ε and c_k are two constants with the considered values of 1.048 and 0.094, respectively, for the present study. The energy equation, which is solved for the internal enthalpy ($h=e+\bar{p}/\bar{\rho}$), is as follows:

$$\frac{\partial}{\partial t}(\bar{\rho}h)+\nabla(\bar{\rho}\tilde{u}_i h)+\frac{\partial}{\partial t}(\bar{\rho}K)+\nabla(\bar{\rho}\tilde{u}_i K)-\frac{\partial \bar{p}}{\partial t}=\nabla\alpha_{eff}\nabla h+\dot{R}_{heat}. \tag{12}$$

where K, α_{eff} and $\dot{R}_{heat}$ are kinematic energy, effective thermal diffusivity and heat generation due to reactions, respectively. The temperature equation for the fluid domain is as follows:

$$\frac{\partial T_f}{\partial t}+u_j\frac{\partial T_f}{\partial x_j}=\alpha_f\frac{\partial^2 T_f}{\partial x_j \partial x_j} \tag{13}$$

where α_f denote the molecular thermal diffusivity.

Solid Region

In the solid region, the energy equation has to be modeled to obtain the evolution of the space-time temperature. The energy equation states the temporal enthalpy change, which is equal to the divergence of the heat conducted through the solid:

$$\frac{\partial(\rho_s h)}{\partial t} = \frac{\partial}{\partial x_j}\left(\alpha_{eff}\frac{\partial h}{\partial x_j}\right), \tag{14}$$

where h is the specific enthalpy, ρ_s the solid density and $\alpha_{eff} = \kappa / C_p$ is the thermal diffusivity which is defined as the ratio between the thermal conductivity κ and the specific heat capacity C_p.

Solid-Fluid Coupling

At the solid-fluid interface, since there is no surface reaction, the temperature continuity ($T_f|_\Gamma = T_s|_\Gamma$) and heat fluxes balance ($Q_f|_\Gamma = Q_s|_\Gamma$) must fulfill the conservation of energy,

$$k_f \frac{\partial T_f}{\partial n} = k_s \frac{\partial T_s}{\partial n} \tag{15}$$

where n, k_f and k_s are representing the normal direction to the wall, fluid and solid thermal conductivity, respectively. Here, a Neumann-Neumann decomposition approach is applied among various available thermal field coupling techniques (Quarteroni and Valli, 1999), guaranty the balance of $T_f|_\Gamma = T_s|_\Gamma$ and $Q_f|_\Gamma = Q_s|_\Gamma$ equations under the prescribed tolerance.

2.2. Model setup and Discretization methods

The solution uses a compressible transient turbulent flow model to include the turbulence mixing and the buoyancy effects in the oven. Table 1 provides details of the employed discretization schemes in obtaining results reported in the current investigation. For the discretization of all terms, second-order accuracy is considered. For the pressure–velocity coupling, the algorithm of PIMPLE, which is a hybrid of the PISO (Issa, 1986) and SIMPLE (Patankar and Spalding, 1983), is implemented in this transient modeling. This algorithm proposed better stability and convergence rate for higher time-step values and stronger coupling applicability using the PISO and SIMPLE for the inner and outer corrector loop, respectively (Pendar and Páscoa, 2019). In the OpenFOAM framework, the wall treatment in the LES turbulence relies on the y^+ value near-wall cells. The dimensionless wall distance is defined as $y^+ = (\mathrm{u}_\tau . \Delta \mathrm{y}) / \upsilon$, where υ, u_τ and $\Delta \mathrm{y}$ are the kinematic viscosity, the friction velocity and the nearest distance to the wall surface, respectively. The utilized wall functions, which are presented in Table 1, be activated only in the $y^+ > 11$ (Liu, 2016).

Table 1. Summary for discretization schemes implemented in the current study.

Discretization	Schemes	Description/comments
Time schemes	Backward difference	2^{nd} order, implicit
Pressure–velocity coupling	PIMPLE	Hybrid of SIMPLE- PISO algorithms
Spatial discretization	Gradient Gauss linear	2^{nd} order (Gaussian integration), Linear interpolation (central differencing)
	Divergence — Gauss upwind	2^{nd} order unbounded (Gaussian integration), Upwind differencing
	Laplacian surface normal gradient — Gauss linear corrected	Unbounded, 2^{nd} order, Conservative
Wall functions	ν_t — nutkWallFunction	Serves as a condition with zero gradient for the modeled k
	K — kqRWallFunction	develops a ν_t near-wall profile using a modeled k

3. Problem Description

3.1. Oven Characteristic and Boundary Conditions

The fluid-solid interaction (FSI) in the curing oven, with the aim of energy-saving and operation optimization, could be computed by using high-order unsteady setup and accurate boundary conditions, flow rates, and temperatures for air nozzles, air panels, and return air ducts located on the walls. A full-length automotive oven, in combination with the traversing BiW, is modeled in the present CFD computation. The oven's external walls are specified as a convective condition to account for heat loss to the ambient air, while the surface of the BiW is determined as having an insulated boundary. The schematic structure of the applied curing oven, including all zones in the heat-up, holding and cooling stages, is provided in Fig. 3. The oven configuration with 53 meters total length has six connected zones, three for the heating up, two for the holding, and one for the cooling process. The current structure is based on an existing automotive oven, and the operating parameters in all zones are validated using actual conditions for the base oven case. The details of each zone's boundary conditions before modification, e.g., the airflow rate and mean temperature of hot/cold re-circulating air components with their physical characteristics, are specified in Table 2. The turbulence intensity (TI) is kept at 2 % for injected heated airflows from all components and the inlet flow from the oven's entry. Air is specified as an ideal gas with the buoyancy forces created by gravity in the negative y-axis. The time step size in all the cases was set at 2.5×10^{-5}, which was small enough to guarantee the Courant number is less than 1.0 and capture the flow details. It was verified that the results are unaffected by the lower Courant number values. The width of the oven at the upper and middle part of the entrance are 2.40 m and 2.65 m, respectively. Also, the oven's height is 2.53 m. A BiW enters the oven, is taken upwards in a lift prior, then transported through the zones on a conveyor with the velocity of V=1.7 m/ min. The lengths of zones 1, 2 and 3 in the heat-up area are 1.2 m, 18.5 m and 10 m, respectively. Also, zones 3,4 and 5 in the holding and cooling regions are 17 m, 1.4 m and 5 m long, respectively.

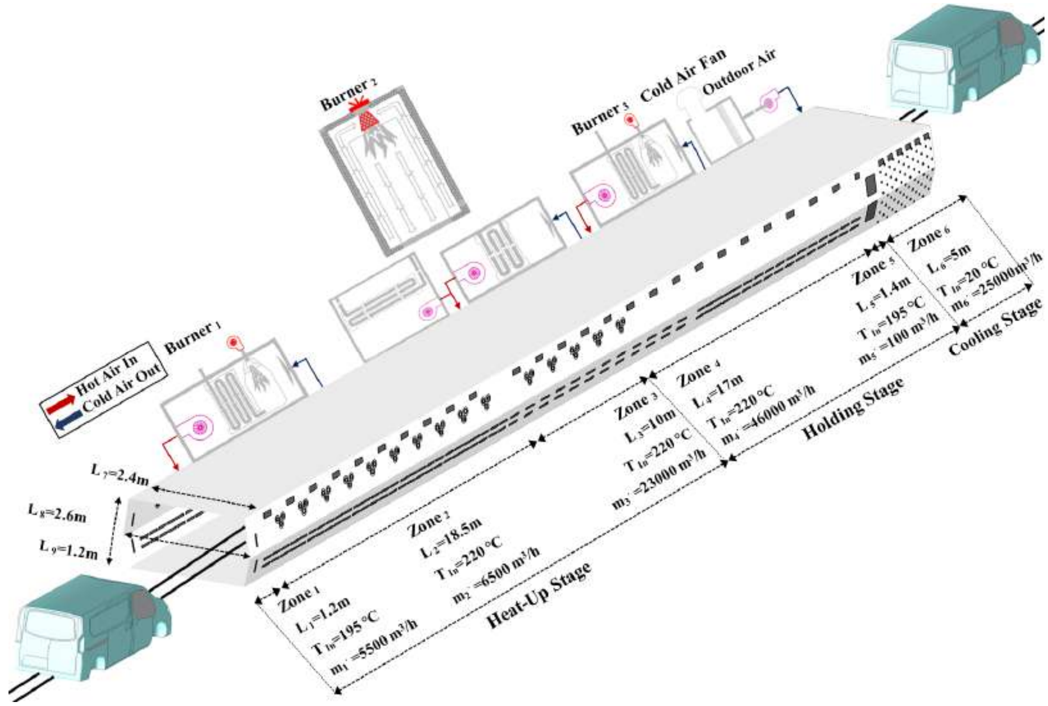

Fig. 3. Schematic representation of the computational domain for a fully configured multi-zoned oven: including heat-up, holding and cooling stages.

These zones are designed to heat the body, maintain a steady temperature without a severe jump, and ultimately cool down the treated BiW. The temperature is raised to the paint solvent vaporization point in the heat-up region, which results in molecular paint curing. The oven in the present study heated the BiW mostly in convection mode. As depicted in Figs. 3 and 4, as well as data from Table 2, hot-air circuits that use heated walls, hot-air nozzles and panels heat the interior of the oven. The heated air is continuously supplied by burners 1 to 3 (see Fig. 3), blown via fan and passes through the tubes, and finally injected into the mentioned components. The supplied hot-air temperatures, which are blown from the wall-mounted nozzles and panels in different zones, ranged from 190 ˚C to 220 ˚C, and the velocities of turbulent flow ranged from ≈ 3.0 m/s to 21 m/s (see Table 2). Relatively cooler fresh air is replenished from two ends of the oven, in addition to the mentioned circuits, to compensate for the lost air. The return air ducts located at the top are evacuated of an equivalent airflow volume in a crosswise direction to the axial direction zone (see Fig. 4), and the outlets are defined as pressure boundaries. In Fig. 5, the car body surface, Citroën Berlingo model, with highliting of aesthetic key lines that include wheelbase, character, accent, waist, and roof lines with the heights of 0.3 m, 0.57 m, 0.88 m, 1.18 m, and 1.81 m, from the ground, respectively, are drawn to use during the analysis of the results.

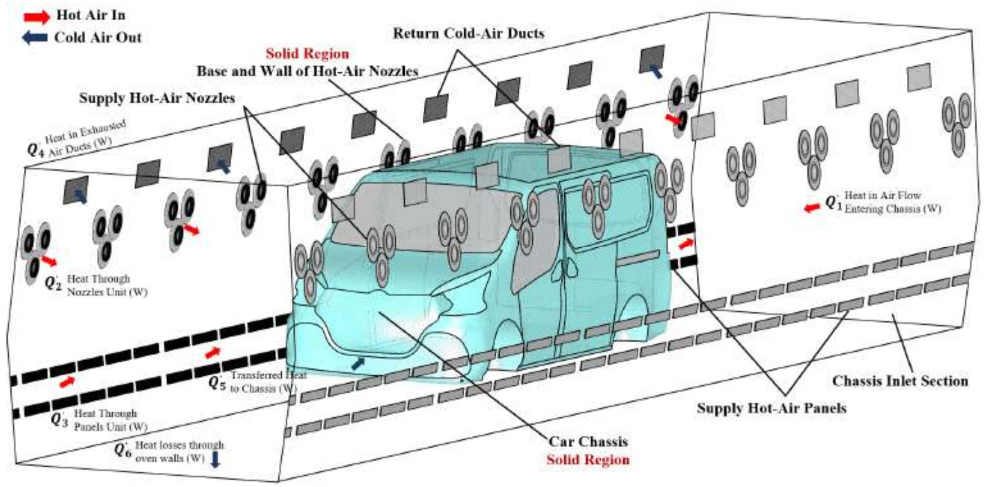

Fig. 4. Schematic drawing of oven's vital layouts boundary conditions: supply air nozzles and panels, return air duct, chassis inlet, and an outlet section.

Table 2. Preliminary geometrical characteristics and operating conditions of the studied oven in the present work.

		Number	Mean Area	Airflow Rate	Mean Air Temperature	Mean Air Velocity	Zone Length
		N	A (m^2)	$\dot{m}$ (m^3/h)	T (°c)	U_{mean} (m/s)	L (m)
Inlet	Natural Air Inlet	1	6.430	7900	30	0.341	-
Zone 1	Upper Hot Air Panel	1	0.074	5500	195	20.57	1.2
	Lower Hot Air Panel	1	0.074	3000	195	11.20	
Zone 2	Hot Air Nozzles	60	0.834	65000	220	3.107	18.5
	Hot Air Panels	108	4.976				
	Return Cold Air Ducts	20	2.155	6500	190	8.377	
Zone 3	Hot Air Nozzles	30	0.417	23000	220	3.477	10
	Hot Air Panels	32	1.787				
	Return Cold Air Ducts	12	1.293	23000	190	5.926	
Zone 4	Hot Air Panels	88	3.810	46000	220	3.353	17
	Return Cold Air Ducts	18	2.048	46000	190	6.238	
Zone 5	Upper Air Panel	2	0.856	100	195	0.2	1.4
	Lower Air Panel	2	0.852	100	195	0.2	
Zone 6	Cold Air Fan	144	0.772	25000	20	11.54	5
	Return Air Ducts	12	0.810	27560	50	9.4325	

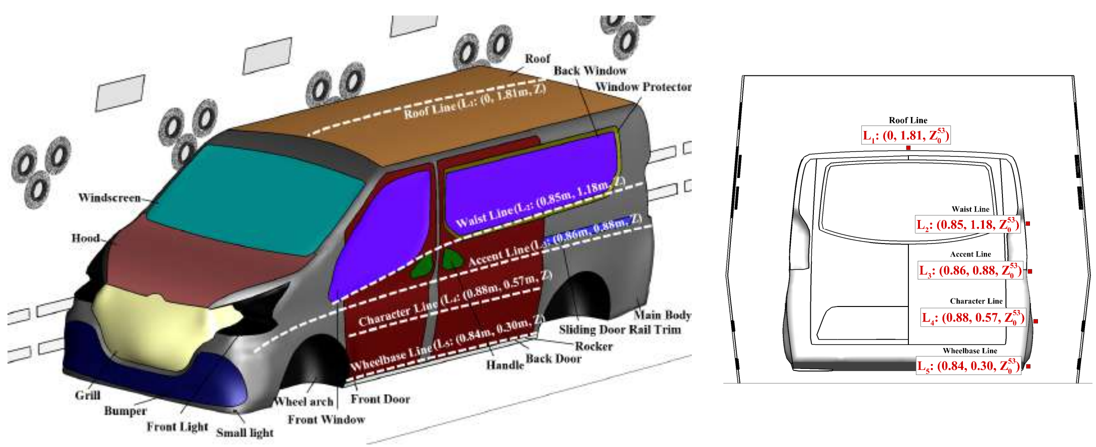

Fig. 5. Schematic reperesentation of vehicle surface, Citroën Berlingo model, with all assembly and aesthetic key lines.

3.2 Description of Optimized Ovens

A summary of the steps involved in designating the modified version of the oven is presented here; see Table 3. These corrections are examined for zones 1 to 3 and 6, where the diffusion of the heated air is implemented through two series of injectors positioned on both the oven's upper and lower walls. For modification in the case Oven_3, the share of the flow rate is manipulated by the equal volume of hot air rate production by means of burners 1 to 3. Around 14.7 %, 4.3 %, 4.3 %, and 10 % of the flow rated is subtracted from the upper channels and added to the lower ones in zones 1, 2, 3, and 6, respectively, compare to the base oven (Oven_1). These manipulations are intended to improve convection at the exact amount of generated airflow rate, which is derived from the burners. In the Oven_2 case, this process is implemented much more compared to the Oven_1 case (base oven) with values of 25 %, 15 %, 10 % and 10 % for zones 1, 2, 3, and 6, respectively.

Table 3. The details of operating conditions for the optimized ovens that are considered in the current study.

		Zone 1			**Zone 2**		**Zone 3**		**Zone 6**		
		Hot Air ($\dot{m}$ (m^3/h))	**Percent**		**Hot Air ($\dot{m}$ (m^3/h))**	**Percent**	**Hot Air ($\dot{m}$ (m^3/h))**	**Percent**		**Cold Air ($\dot{m}$ (m^3/h))**	**Percent**
Oven_1 (Base Oven)	Upper Hot Air	6372	75%	Nozzle	16246	25%	6900	25%	Up	9997	40%
	Lower Hot Air	2124	25%	Panel	48744	75%	20698	75%	Down	14997	60%
Oven_2 (Modified_1)	Upper Hot Air	4266	50%	Nozzle	6480	10%	5396	15%	Up	14997	60%
	Lower Hot Air	4266	50%	Panel	58464	90%	23457	85%	Down	9997	40%
Oven_3 (Modified_2)	Upper Hot Air	5497	64.7%	Nozzle	9325	14.3%	5225	19.3%	Up	12500	50%
	Lower Hot Air	2998	35.3%	Panel	55656	85.7%	22372	80.7%	Down	12500	50%
Mean Air Temperature	195 °C			220 °C			220 °C		50 °C		

3.3 Computational Grid

The computing grid quality directly influences the accuracy of the numerical results. A comprehensive representation of the computational grid for a considered full-length curing oven with multiple close-up views is depicted in Fig. 6. Despite considerable complexities, all zones of the computational domain, solid and fluid regions inside the oven, are constructed using fully structured quadrilateral grids. Except for cases including the traversing box of the car body, comprising non-uniform tetrahedral cells due to the complex geometry.

The computational domain is decomposed into fifty-four sub-sections over the six zones, with their components, to achieve more control on the grid's ratio and size, especially in regions with higher flow gradients, i.e., near the nozzles, panels, ducts, and fans. The wall grid size near boundaries significantly affects the conjugate heat transfer (CHT) predictions, as in Reynold's analogy. To perform a mesh independence analysis, four grids with various resolutions and volumetric mesh counts of the coarse_1 (≈ 25.5 million cells), coarse_2 (≈ 32.5 million cells), medium (≈ 39.2 million cells), and fine (≈ 47.75 million cells) were produced with suitable values y^+ in all grids to adequately capture the boundary layers. Based on the grid convergence evaluation (see Fig. 7) for the mean temperature distribution along the roof-line (L_1) of considered four different grid sizes in zones 3-6, we concluded that modeling using the medium mesh with an overall account of ≈ 39.2 million cells is appropriate. It is clear that increasing the surface cells makes the difference between the mean temperature values negligible.

For this grid, the number of cells used in the streamwise (n_ξ), vertical (n_η), and spanwise (n_ς) directions are around 2177, 156, and 92, respectively (see Fig. 6). At the boundaries of nozzles, panels and ducts located on the walls of the oven, the mesh comprises a prism layer with a height of roughly 1.6×10^{-3} m (medium mesh). The size of the grid progressively increases with a higher ratio outward of the mentioned boundaries, where the flow variations are comparably reduced. Despite the oven's five hundred and nineteen components (see Table 2), the mesh size near the wall and features specified and tweaked, a mesh with suitable values of y^+ was constructed.

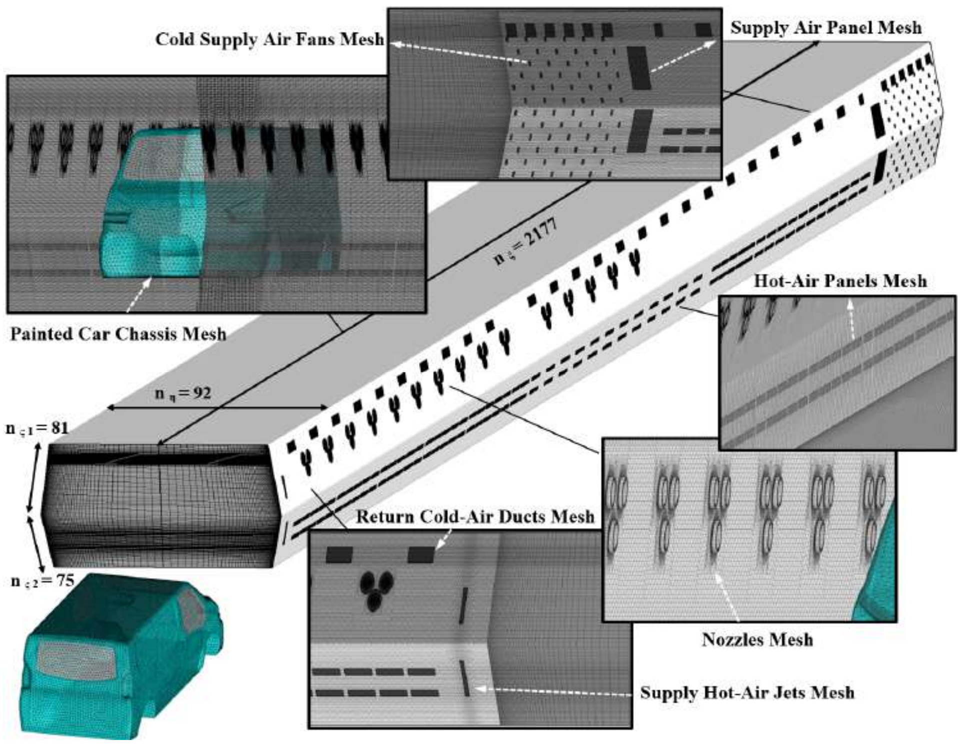

Fig. 6. Generated 3D structured grid distribution over the full oven's computational domain.

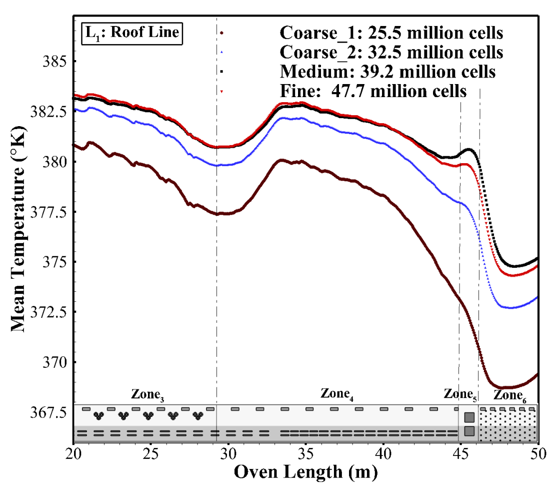

Fig. 7. Considering the effect of four various grid resolutions implemented for a grid dependence test based on the mean heated air temperature in zones 3 to 6 (Δt= 240 s).

3.4 Validation

In this part, for validation, the accuracy of the utilized CHT code and numerical method were assessed by modeling transient heat convection-conduction in the 3D heat sink problem, the most comparable to the present work, automotive curing oven, in terms of the fluid-solid interaction (FSI) flow physics that actually occurred. Fig. 8 depicts the computational domain's dimensions and boundary conditions. The squared domain has a 600 mm side length, around 43 times the heat sink's height, and all-around surfaces are subject to atmospheric pressure conditions. The heat sink's base is heated to a constant temperature (T_{hot} [$^{\circ}$k]). The fully structured grid generated in this instance comprises ≈ 8.6 million cells after evaluating various grid sizes (see Fig. 9). All grid sizes in various directions of the domain and over the heat sink surface are reported in Fig. 9.

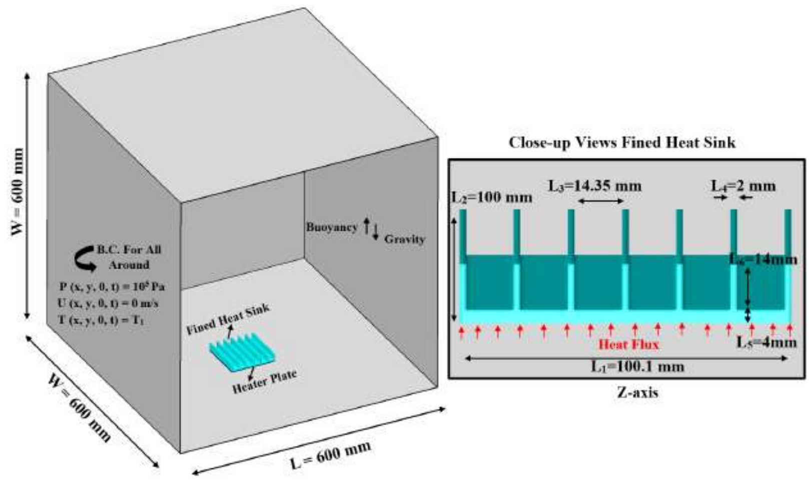

Fig. 8. Representation of the heat sink as a validation case, 3D configuration dimensions and boundary conditions.

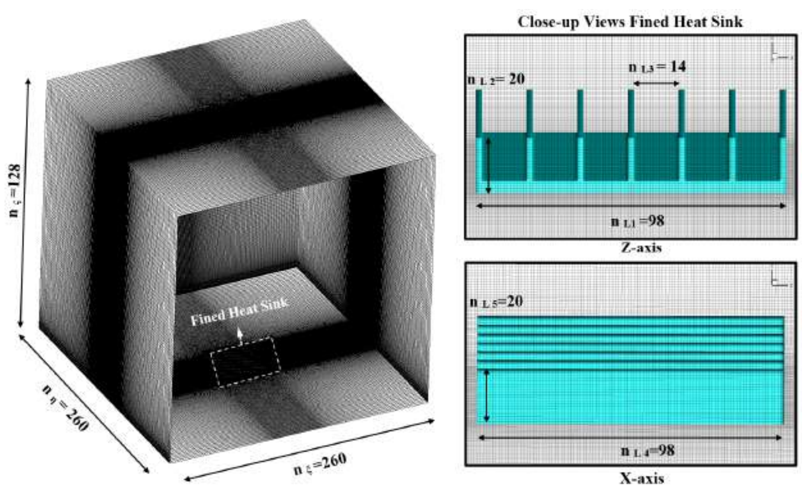

Fig. 9. Visualization of the structured grid distribution over the computational domain and heat sink surface.

The heat power conditions for five considered cases are described in Table 4. T_∞ and T_{hot} are indicated as the mean atmospheric and central fin base temperatures, respectively. In Fig. 10, the average heat transfer ($\bar{h} = q''/T_{hot} - T_\infty$) and Nusselt number ($\overline{Nu} = \bar{h}.l/k$) values are validated with the experimental data of da Silva et al. (2019) and the analytical results of Harahap and Rudianto (2005). k, q'' and l are the fluid thermal conductivity, heat transfer flux among the fluid and heatsink and half of the fin width ($l = L_2/2$). The $\overline{h}$ and $\overline{Nu}$ values are computed through using the NusseltCalc tool (Magnusson, 2010). The generated heat by the sink is conducted to the fins and exchanged via mostly convection mode to the surrounding fluid, increasing its temperature gradient. Less than 7 % error among the obtained current studies results, and experimental and analytical data proof a good agreement (see Fig. 10). This agreement guarantees the reliability of the present CHT code under the OpenFOAM framework in curing oven solving.

Table 4. Summary of the cases temperature settings implemented in the current work.

Cases	A	B	C	D	E
T_∞ [°k]	295.94	296.29	295.63	297.16	295.45
T_{hot} [°k]	304.30	310.92	322.07	348.32	369.26
ΔT [°K]	8.36	14.63	26.44	51.16	73.81

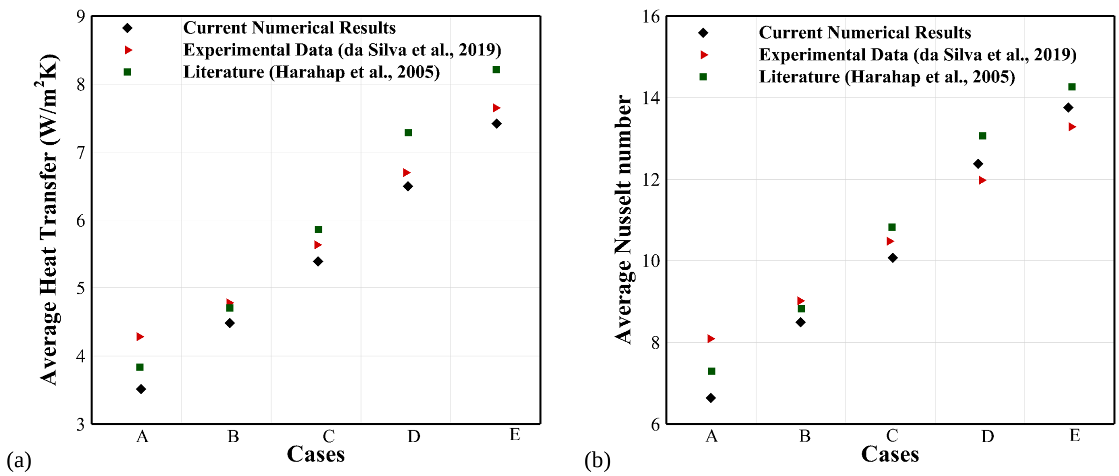

Fig. 10. The conjugate heat transfer solver validation for various heat sink geometries: Comparisons of computed (a) average heat transfer coefficient, and (b) average Nusselt number (t = 5 s), with the experimental data (da Silva et al., 2019) and literature (Harahap and Rudianto, 2005).

4. Results and Discussions

This section intends to analyze the time-averaged characteristics of the car curing process during the electro-deposition painting stage. Precise details can be obtained from the results of this unsteady simulation – such as high-resolution flow distribution in different zones of the oven, diffusion patterns and mixing streams produced due to various injected air streams, the convective heat transfer rate, vortical structures topology, velocity, and temperature map on the car body. Data and structures of available PSA Mangualde automotive curing oven's PaintShop plant and real Citroën Berlingo car features are considered for optimization-based analysis.

4.1 Heat transfer

The objective is to analyze the mean air temperature along with the oven length, together with precise temperature distribution obtained on the solid car body surface. As mentioned earlier, the accurate LES turbulent model is used in the current simulation to achieve this goal. Figures 11 and 12 show the complexity of the hot-air flow field pattern, mean temperature distribution, in the center and side section planes during the full oven length. Nine consecutive frames of temporal variation of the mean air temperature during one complete cycle, up to reaching the fully operated condition after startup of the base oven (Oven_1), is presented in Fig. 11. Analyzing these frames is capable us to comprehend the complex initial hot-air flow interference to the oven space, which is difficult in practice. In zones 1 and 2, the heat-up stage, hot-air feeding is accrued with the convection and circulation thermal heat transfer. A weaker hot-air operation and the lower average temperature in the third zone of the heat-up stage are clear because of low panel density. The facts of inappropriate diffusion directions of the hot-air injectors during the heating process (Fig. 12a) depict the necessity of proposing an optimal oven to reach the homogenized proper temperature distribution. As apparent in Figs. 11, 15, and 16 for the case of Oven_1, due to the slight hot-air gradient and density in the locations where car bodies are traversing, less thermal power is absorbed via convection between the solid car surface and the oven's gases. To address the issue of weak heat diffusion and dispersion in the upper-wall and lower-ground regions where the roof-line and wheelbase-line are located, especially in zones 3 and 4, the Oven_3 case is introduced. By moderate redirection of the hot air injectors and developing flow share of them (see Table 3), the distribution was optimized. The temperature contour in the Oven_3, during all zones, shows a higher uniform distribution, essentially devoid of a severe jump, as well as a gradual longitudinal gradient (Fig. 12c). In the case of Oven_2, the improvement happens, but not precisely in the location that the bodies are traversing, as well as in Oven_3.

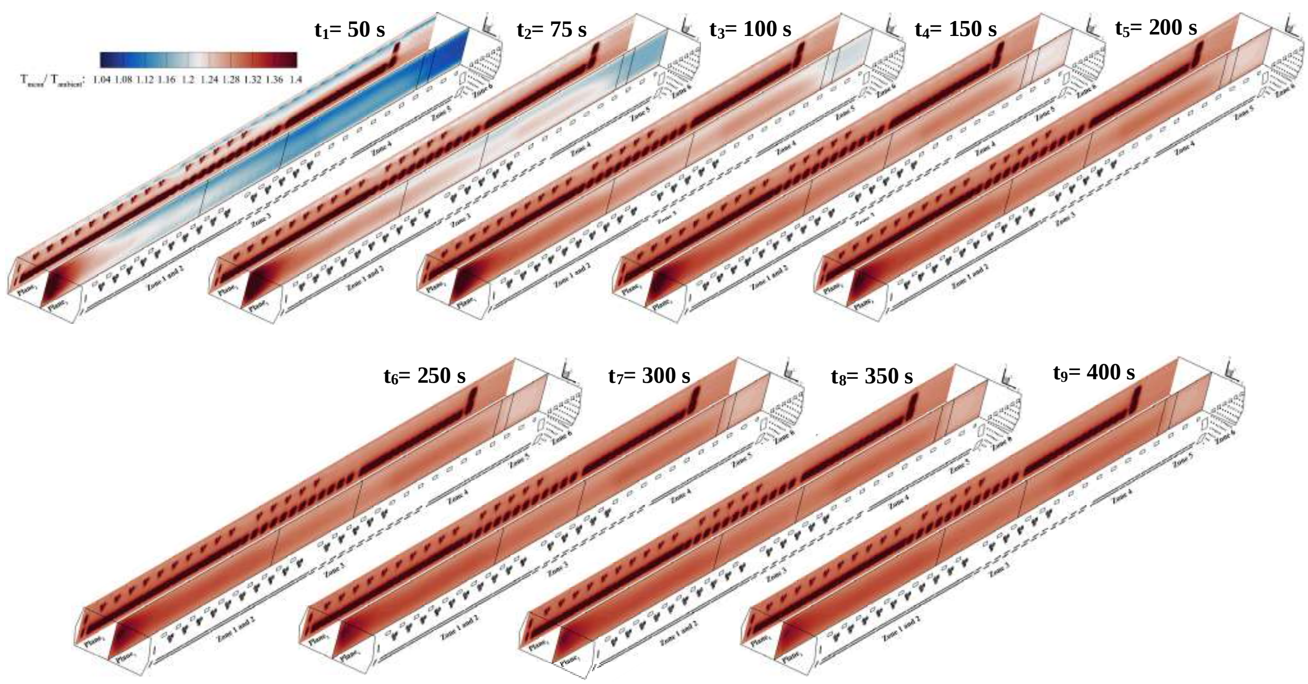

Fig. 11. Time evolution of the mean air temperature, on the center and side planes, along with the full oven length (L= 53m), Oven_1 (Base Oven), vertical lines separated the heat-up, holding, and cooling stages.

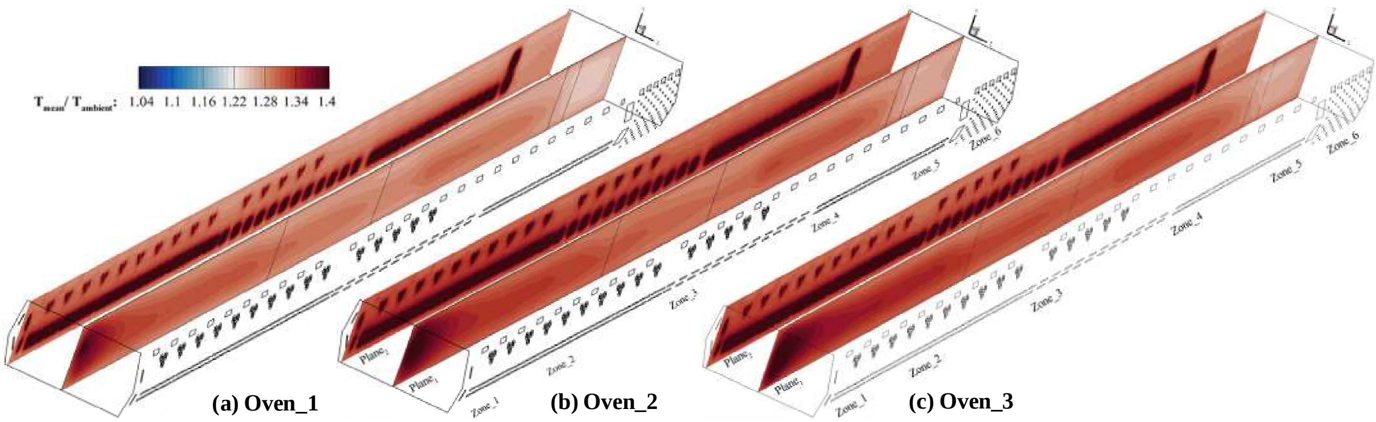

Fig. 12. Mean air temperature on the center and side planes along the entire length of the oven after t= 240 s: (a) Oven_1, (b) Oven_2, and (c) Oven_3.

All phenomena, including forced convection heat transfer between the hot-air and body, conduction heat transfer inside the car body, and radiation heat transfer between oven and vehicle, were modeled with the operated algorithm. These valuable data can be employed for investigating the occurrence of paint film defects during the drying/curing process. Figs. 13 and 14 illustrate the vehicle surface temperature during the heat-up, holding, and cooling stages in one cycle of the oven's operation for the modified case of Oven_3. The values of the calculated temperature, local heat-up gradients, and heat transmission on the car's external surfaces at the locations of the waist, accent, and character lines are observed to be innately high. Being in the vicinity of the hot-air inlet nozzles and panels strike locations, which affect the body by the large size of the recirculation air generation, is the reason. Furthermore, the complex structure of the car body's outer-shell intensifies the temperature distribution's non-uniformity. Despite the fact that the temperature of the body surface in the first half of the oven is lower than the rest, the power absorption in this region by car is higher due to convection and a more significant thermal gradient. Lower and more uniform temperature values were found in portions inside the vehicle. Except for the car body's transverse middle region, where far from the nozzles and panels impinging point, the final distribution in the latter two zones was relatively constant throughout the body surface.

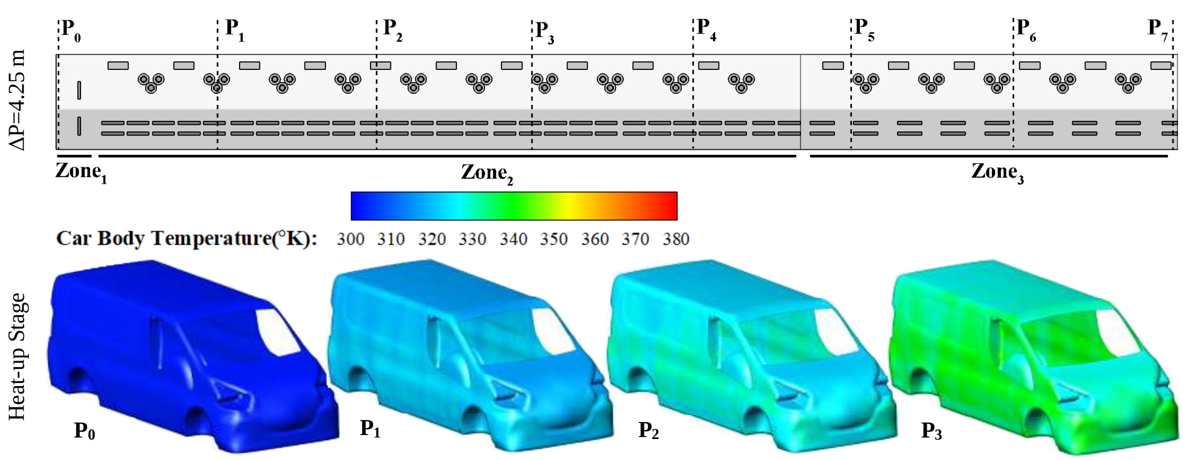

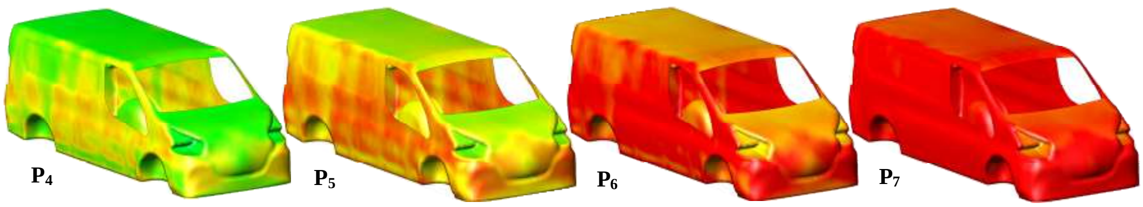

Fig. 13. The calculated temperature visualization through the car body surface at various time instants and oven locations in the heat-up stage (zones 1 to 3), Δt_1=17.5 min, case Oven_3.

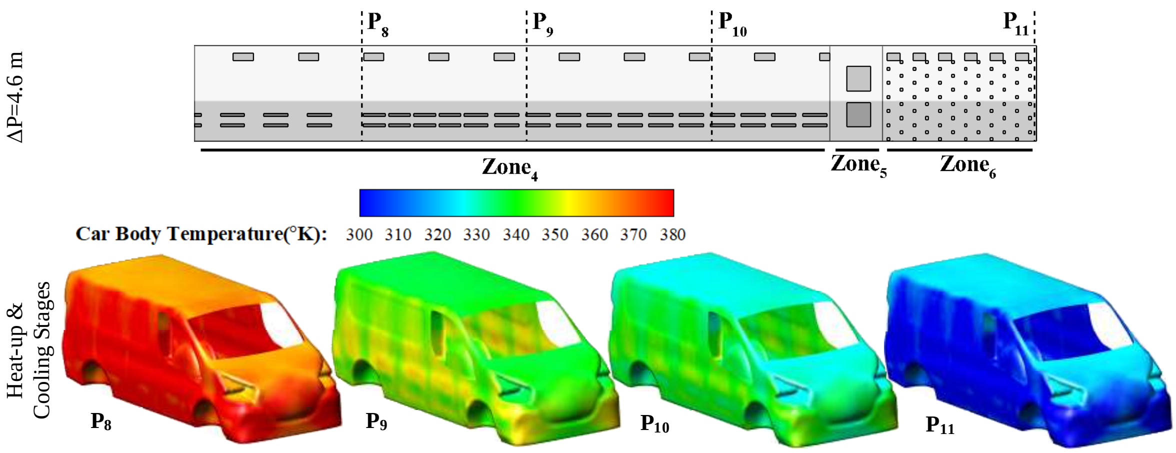

Fig. 14. The computed temperature description on the car body surface at different time instants and oven locations in the holding and cooling stages (zones 4 to 6), Δt_1=13.5 min, case Oven_3.

The mean air temperature distribution, along with the mentioned aesthetic key lines, in a cross-section of the oven center, for three designed ovens are evaluated in Figs. 15 and 16. As evident in the graphs, the overall mean temperature patterns obtained from three modeled ovens are almost reasonably similar and logically accurate based on the actual requirements. In Fig. 15, the severe initial jump in the first zone, which was influenced by large-size panels with a high flow rate, consumes a high amount of energy. The actual reason for this intense increment is to preheat the air to raise the car body temperature, which has a surface with a low outside environment temperature (303 $^{\circ}$k), to reach more quickly to almost equivalence temperature of the initial phase of the oven tunnel. The distribution slope remains almost stable at the holding stage before descending at the cooling stage. As no substantial longitudinal mass flows exist, each zone has a roughly uniform temperature with just some longitudinal variation. The distribution in the base oven (Oven_1) evidences some instability, oscillation, and design weaknesses, which are optimized in the case of Oven_3. In the case of Oven_3, flowrate adjustment, and hot-air diffusion re-direction are implemented with the aim of proper conduction heat transfer.

As the mean temperature distribution shows in Figs. 15 and 16, the adjustment in the case of Oven_3 results in a better hot thermal flow pattern that is precisely directed toward the coated car body surface, causing higher conjugate heat transfer (CHT) without incurring additional costs or using a larger amount of energy. In Fig. 16, all temperature distribution patterns at the waist, accent, character, and wheelbase lines exhibit fluctuating patterns, with peaks associated with the outlying areas where nozzles and panels are located. It is so important to notice that the amplitude of these oscillations is not severe to seriously (maximum ≈ 5 $^{\circ}$k) affect the homogeneity of the paint film during curing process. The amplitude that looks extremely large as the oven's whole length (53 m) is compressed in these frames.

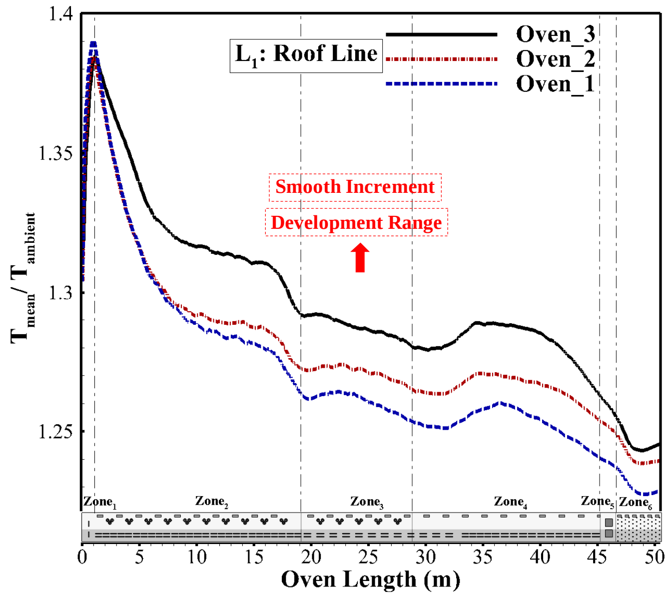

Fig. 15. Comparison of dimensionless temperature values distribution for the three considered cases of base and modified ovens (Oven _1 to Oven _3) at the roof-line location, t= 240 s.

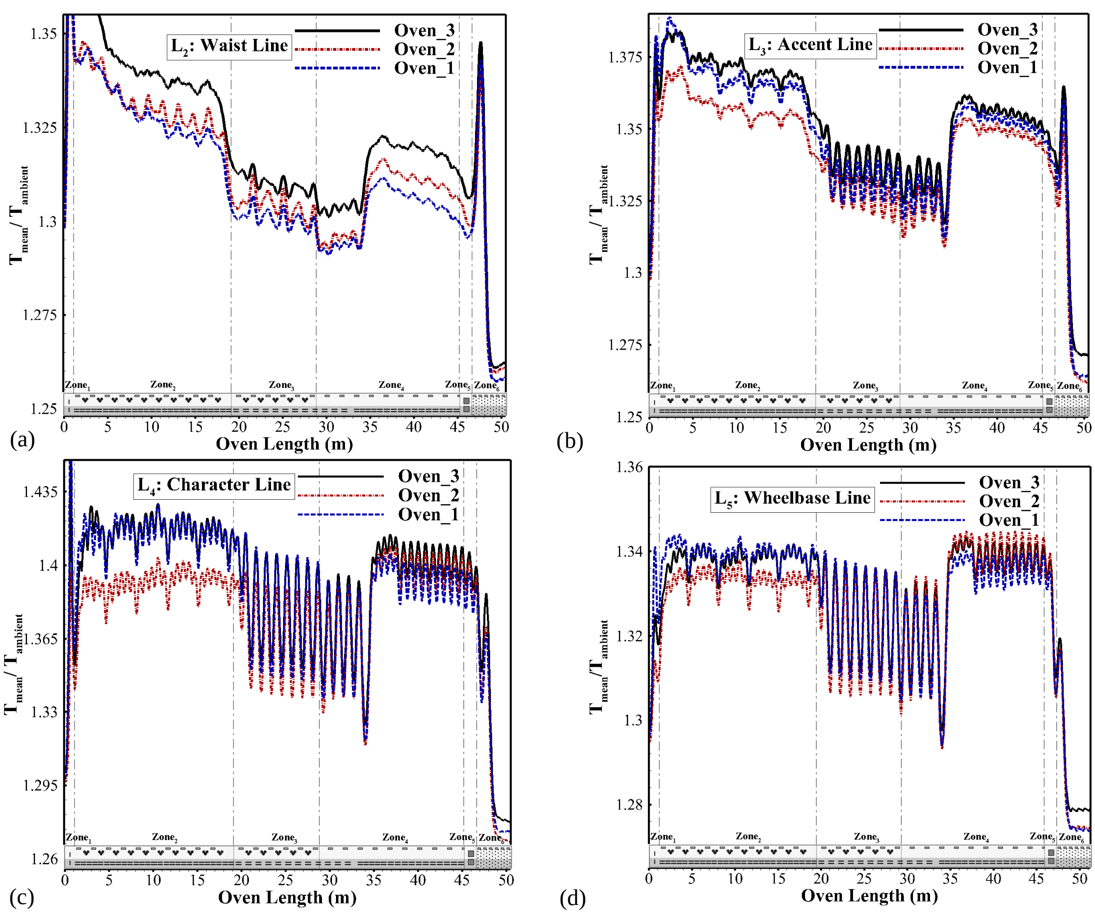

Fig. 16. Assessment of non-dimensional temperature values distribution for the base and modified ovens cases (Oven _1 to Oven _3) at the: (a) waist-line, (b) accent-line, (c) character-line, and (d) wheelbase-line location, t= 240 s.

The temporal history evolution of the dimensionless mean air temperature at the roof-line for the Oven_3 case, along with the full oven length, is also presented in Fig. 17. The overall qualitative behavior of the computed temperature distribution curves for various times satisfied what is expected from an automotive curing oven. As evident in Fig. 17, the temperature distribution along the length of the oven has not significantly changed and reached a constant fully-operated state after Δt=≈ 300 s from the start-up point, where the vehicle paint curing process began to run. The lines in around t ≥ 300 s indicate a smooth and stabilized distribution after experiencing fluctuating and unstable distribution in around t ≤ 200 s during the growing level.

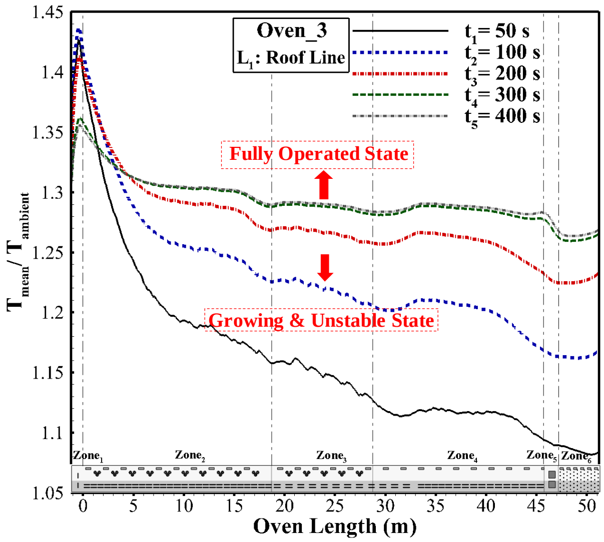

Fig. 17. The temporal history of the dimensionless mean air temperature (°k) at the roof-line for the Oven_3, along with the full oven length.

To deeply analyze the interaction between the solid body and injected fluid, Fig.18 presents the hot-air temperature contour of seven cross-section planes at different longitude positions over the vehicle body surface. In the middle of the heat-up and holding stages, where the panels, nozzles, and return air ducts are located. The transmission heat transfer is significantly higher around the nozzles and panels district heat sources on the exterior surfaces of the body. The maximum temperature take place at the character-line, near the heat source of the panels, which can be managed. In Fig. 18b, the temperature ranges due to the absence of nozzles in the oven's upper side are moderate compared to the heat-up stage. In the holding stage, the corresponding air temperature distribution is more uniform than all planes'heat-up stage.

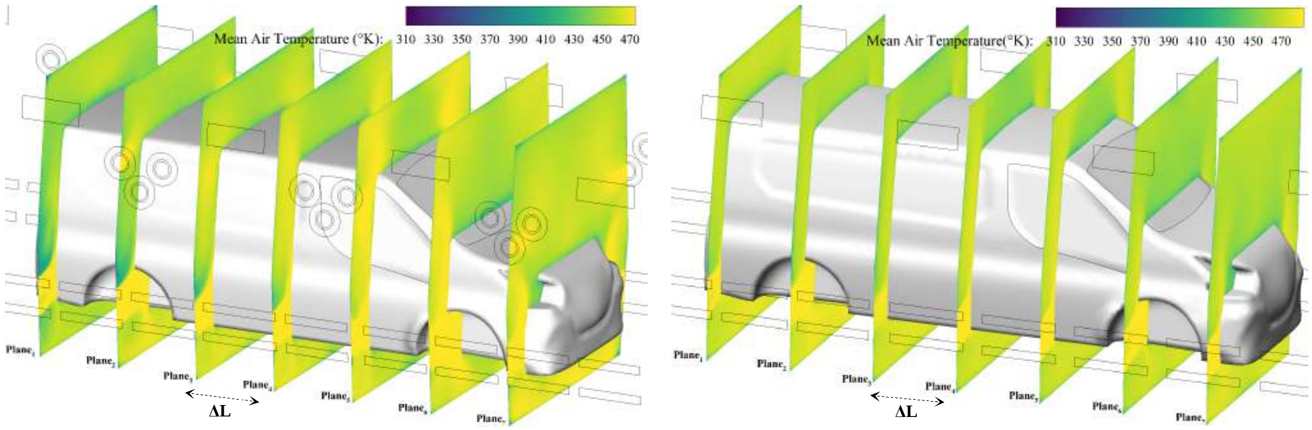

(a) Heat-up Stage (b) Holding Stage

Fig. 18. Air temperature contour demonstration of seven 2D planes (ΔL= 0.75 m) at various longitude locations over the car body surface in the middle of the (a) heat-up and (b) holding stages, Δt= 240 s.

Fig. 19 depicts the mitigated/exceeded temperature regions, on the car surface during traversing inside the modified oven (Oven_3), below/above the minimum and maximum recommended ranges in the curing window represented in Fig. 1. It is evident that the areas between the waist and accent lines are overbaked/burned-out. Additionally, it can be found that the car's hood, rear parts of the roof, and small back areas of the floor remain under-baked. The temperature contour on the car surface during the heat-up curing stage proves that the body's hood, roof, and door areas need more attention compared to other regions. Our results show the modification in diminishing the under-baked areas in the lower parts of the car body. This defect is solved by the panels and nozzles hot airflow redirection in case Oven_3. The curing can be fully organized with little attention to the detected problematic areas.

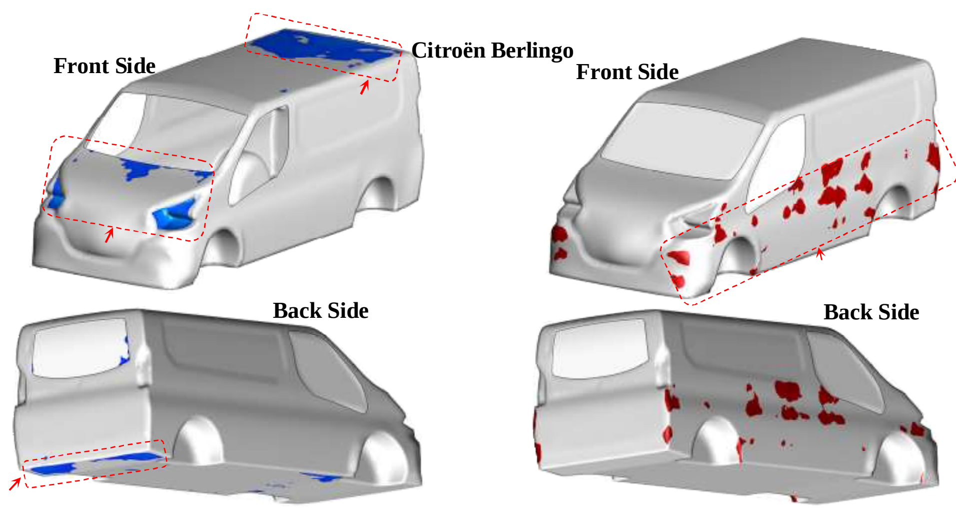

(a) Regions prone to be under-baked (b) Regions prone to be over-baked

Fig. 19. Detected locations prone to the over-bake and under-bake phenomenon obtained support to optimize hot-air injection patterns via nozzles and panels, case Oven_3.

4.2 Flow Characteristics and Vortical Structures Topology

In Fig. 20 to Fig. 27, the fluid dynamic characteristic details about the velocity field, mixing of different injected air streams from components, and detected air circulation structure/nature in different regions of the oven and on the car body surface are discussed. The comparison of the mean air velocity distribution across the center and side planes along the entire length of the oven for three considered scenarios in this work is presented in Fig. 20. As a superior of all considered cases (Oven_1 to Oven_3) is the low-speed hot-air diffusion during the interaction with the car body surface in the heat-up and holding stages. Except for the hot-air velocity at the oven’s entrance, that have slightly higher values when hitting the body surface (zone 1). This benefit allows the coated car body to exchange heat at the proper time and velocity while traversing the oven’s length. This results in the paint film forming smooth, unblemished, aesthetic appeal with higher quality. In contrast to other stages, the cooling region experiences a higher velocity range. But it causes no distortion or destructive consequences on the formed paint film quality, which is almost dried/cured car bodies passing through this stage. In Oven_3, the velocity distribution exhibits greater value in the car traversing location, mainly in the holding stage, compared to Oven_1. More efficient conjugate heat transmission results from this enhancement. The maximum range of difference in velocity magnitude values between cases is ≈ ≤ 0.28 m/s (see Fig. 22a), which is not sufficiently harsh to influence the homogeneity and uniformity of the paint film significantly.

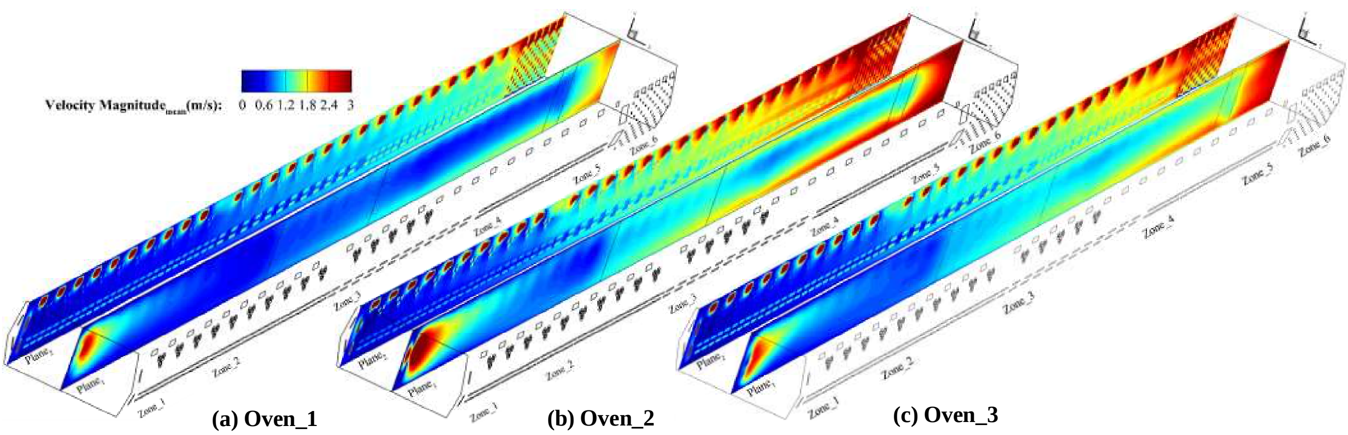

Fig. 20. Comparison of the mean air velocity contours between the (a) Oven_1, (b) Oven_2, and (c) Oven_3 cases, during the oven all zones, at the center and side planes, t= 240 s.

The mean air velocity contour at seven various sections, where the car body is placed in the middle of the heat-up and holding stages, is illustrated in Fig. 21. The critical location of the considered planes, where the oven's components are presented, for velocity magnitude examination is applicable. In order to prevent paint distortion and preserve visual appeal quality, the oven’s components were designed to inject air into the vehicle surface at a low and optimum velocity. The thrown air flow reaches the body surface with limited velocity even in nozzles longitude distance, particularly in the holding stage (see Fig. 21).

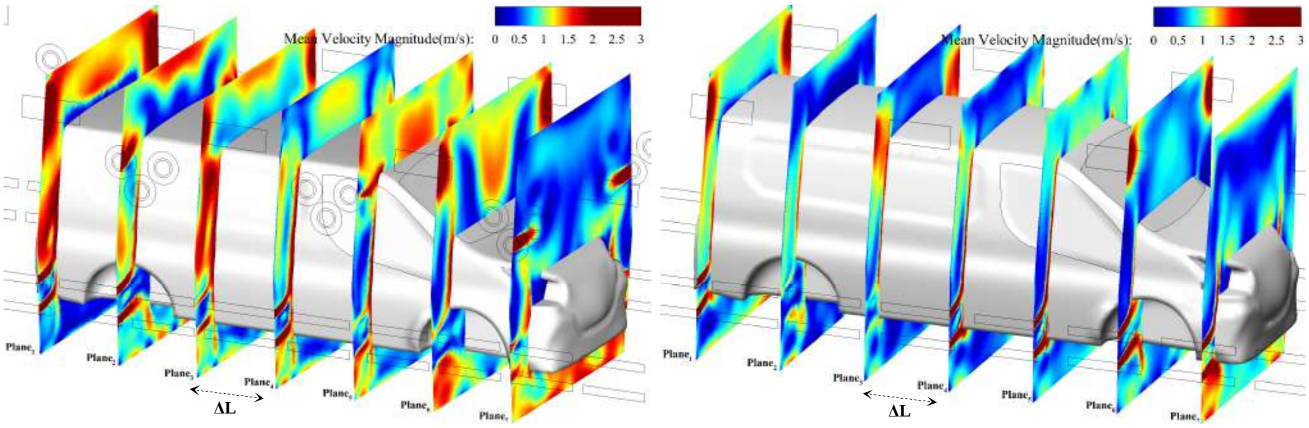

(a) Heat-up Stage (b) Holding Stage

Fig. 21. Mean air velocity contour visualization of seven planes (ΔL= 0.75 m) at different longitude locations over the car body surface at the middle of the (a) heat-up and (b) holding stages, Δt= 240 s.

in Figs. 22a, the mean air velocity along the roof-line, in a cross-section of the oven center, for three designed ovens are evaluated. In all cases, a considerable number of oscillations in zones 2, 3, and 4 with a sinusoidal pattern are discernible. The maximum peak-to-peak values of these oscillations are just ≈ 0.03 m/s, which are sufficiently weak to have a noticeable impact on the paint film homogeneity. The intermittent presence of nozzles and panels is the source of these fluctuations. For the velocity distribution over the oven length during various zones, Oven_3 yields a higher and more consistent value.

The temporal evolution record of the mean air velocity at the roof-line for the Oven_3 case, along with the full oven length, is considered in Fig. 22b. Turbulent and chaotic flow occurs at the oven's start-up operating phase, demonstrating higher velocity values. The fully operated states with lower, smoother, and optimum velocity distribution values are happening for the time around t ≥ 240 s.

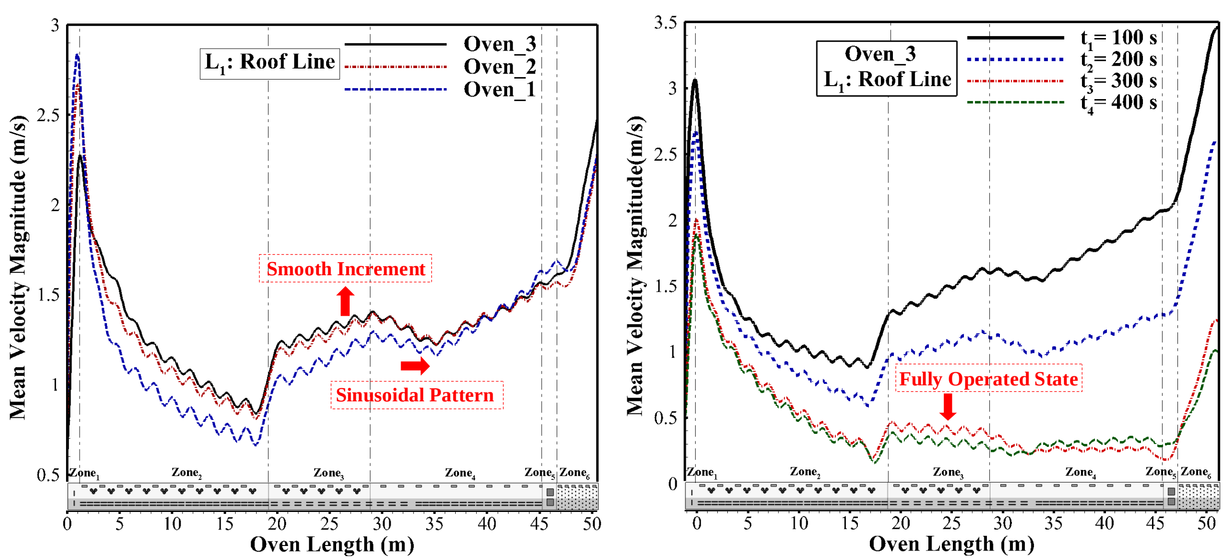

(a) (b)

Fig. 22. (a) Comparison of mean air velocity values distribution for three considered cases (Oven _1 to Oven _3), and (b) time evolution history for the Oven_3, at the roof-line location.

Figs. 23 shows the velocity distribution on the body of Citroën Berlingo in the middle of the heat-up and holding stages. These frames significantly help recognize the mechanisms of the fluid and solid interaction in which range of velocity that can help to have curing implementation with uniform distribution. The car side walls and bumpers are faced hot-air flow with higher ranges (≈ 2.5 m/s). But, almost other regions of the body experience moderate flow velocity values (≈ 1.0 m/s). This defect in the discontinuous velocity distribution can be significantly improved by including hot-air panels with a very low density in the upper and bottom sides of the oven length.

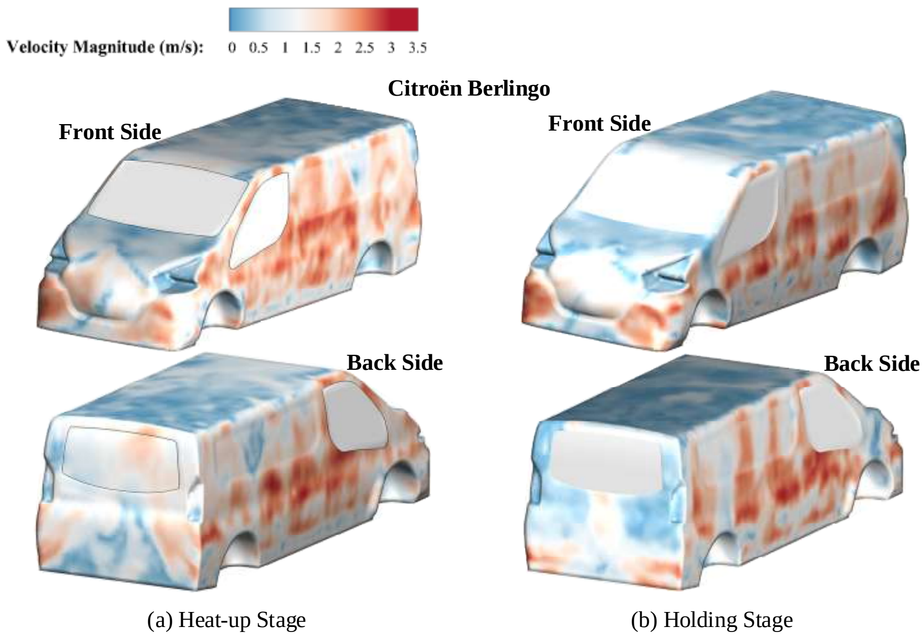

Fig. 23. Calculated vehicle surface velocity at the central locations of the oven in the (a) heat-up and (b) holding stages, case Oven 3.

Fig. 24 illustrates the turbulent kinetic energy (TKE) distribution at the roof-line and accent-line locations for three considered cases in this paper. Two frames show that the turbulent kinetic energy in the case of Oven_3 is lower compared to others, which is an excellent sign of achieving less film distortion and non-uniformity. Proper and gentle heating and curing of the paint film happens there. The flow interaction during the mixing process directly affects their trajectory and structure. This interaction procedure is optimized in Oven_3 and achieves a reduced TKE level.

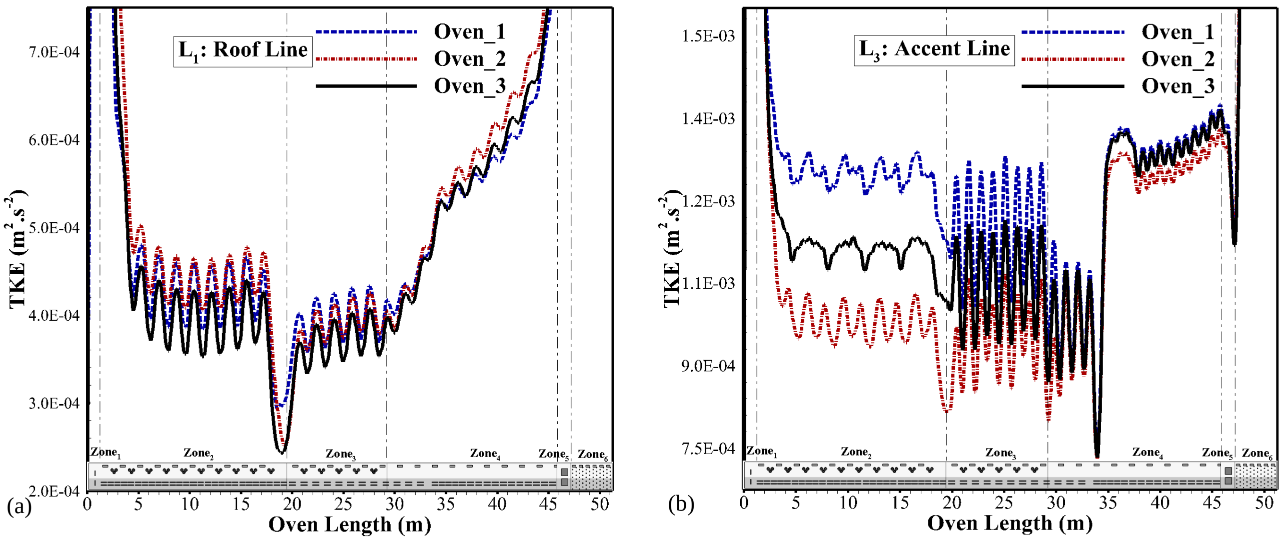

Fig. 24. Turbulence kinetic energy (TKE) distribution plotted in the position of the (a) roof-line, and (b) accent-line, for various ovens, t= 240 s.

Precise detection of the vortical structures and flow streamlines pattern plays a vital role in accurate optimization-based redesigning and effective parametric modification in an automotive curing oven. Here, the LES exact turbulence model is used to meet this requirement. The air vorticity magnitude contours and distributions for three distinct ovens taken into consideration in the current investigation are shown in Figs. 25 and 26. The vortex dynamics are slightly different for cases, and the Oven_3 achieves a larger improvement with a moderate vortical flow covering the car traversing path. The generated momentum at a proper place convects vortices towards the car surface for better thermal homogeneity. The large vortical structures originated from the panels, nozzles and fans, directly influencing how heated air deals with the body surface (during the warm-up and chilling processes) and, consequently, curing performance and paint film quality. The mentioned vortical recirculation structures grow the diffusion efficiency through a tight distance between the components on the wall and the solid traversing body. In the Oven_1 and Oven_2 cases, a severe impact on the upper and lower half of the oven's height happens, which needs more attention. In other words, the modified turns sketch from the lower half components of the oven is intensified and causes more elevated body surface coverage and efficient conjugate heat transfer (CHT) (see Fig. 25c). The congestion of the streamlines at two ends of the oven, i.e., zones one, two and six, supply the greatest impact on the body surface.

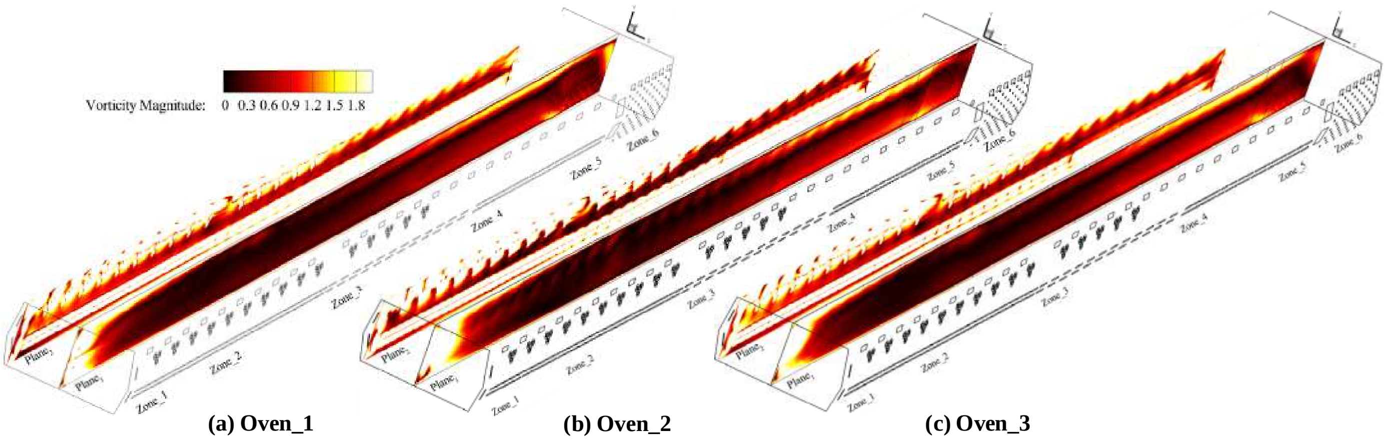

Fig. 25. Comparison of the air vorticity contours between the (a) Oven_1, (b) Oven_2 and (c) Oven_3 cases, during the oven all zones (L= 53 m), at the center and side planes position and time (t= 240 s).

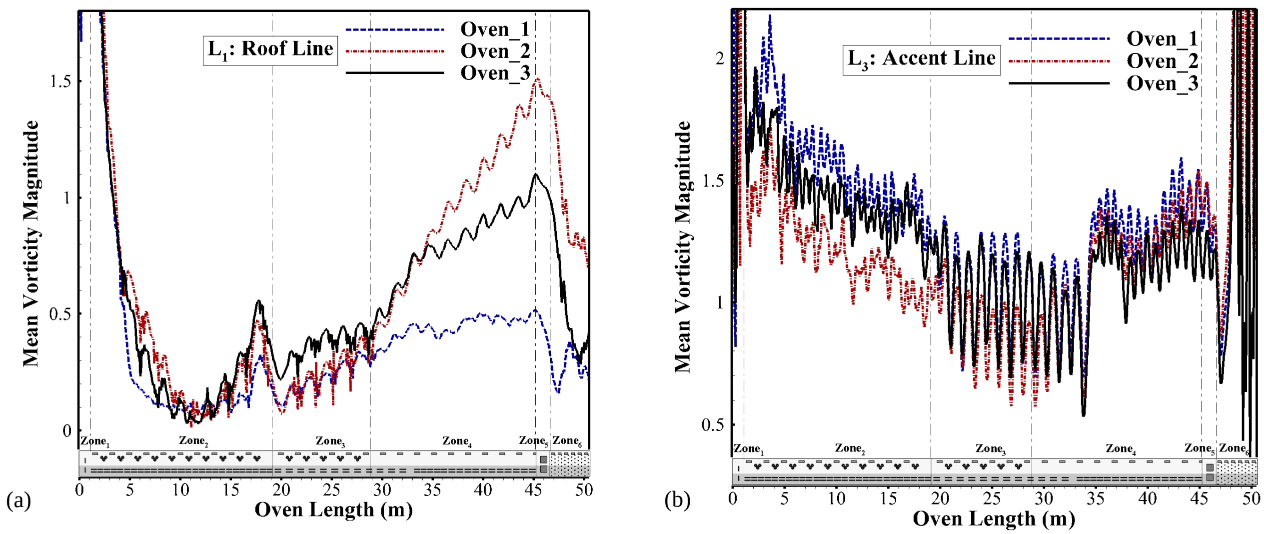

Fig. 26. Vorticity magnitude distribution plotted in the position of the (a) roof-line, and (b) accent-line various oven designs.

Figure 27 visualizes the vortical structures, diffusion pattern and convective flow of the hot-air outlet stream inside the oven. The vortex-growing structures and flow stream near the components of the oven that forced the hot-air flow to change, with regard to velocity magnitude are presented in Fig. 27a. The Line Integral Convolution (LIC) approach is utilized to visualize streamlines (Stalling and Hege, 1997). These patterns are captured at the initiation of a continuous curing operation (t=150 s) before fully mixed chaotic flow steam occurs. These qualitative evolution analyses provide valuable data and aids in better flow control to reach higher transfer efficiency in new optimized redesigned oven. With moderated velocity values, the flow is more controllable by manipulating the flow share and direction of the oven's upper and lower components, which is implemented in this work. The flow type inside the oven is three-dimensional (3D), with large vortices and complex patterns. The circulation of air toward the center point of the oven from the beginning and ending points of the oven due to the operational mechanisms of the ventilating lids is clear. The recirculation zone length (L_{rz}) in the cooling stage is smaller with higher succession of small-scale than the heating and holding stages, which all satisfies the necessity of the curing process. The values of L_{rz} in curing zones are large enough to reach the body surface in the real operational conditions.

The 3D time evolution maps for the second invariant of the velocity gradient tensor (Q) of the LES results obtained from the chaotic stream flow pattern due to multi-directional hot-air flow loading from five hundred and nineteen components of the entire oven are visualized in Fig. 27b. This loading strategy significantly altered the product paint film's quality. This criterion is most commonly used to highlight the vortical structure and efficiently aid in examining the effect of diffusion flow rate and direction on the vortical system and flow discipline in one look. In the t= 150 s of Oven_3, sizable, uniform tubes without any distortion and longitudinal direction shape almost reach the oven's middle formed in heat-up and holding stages. But at the cooling stage, a finer and denser vortex tube with a non-uniform surface is visible, which causes no problem in paint film quality.

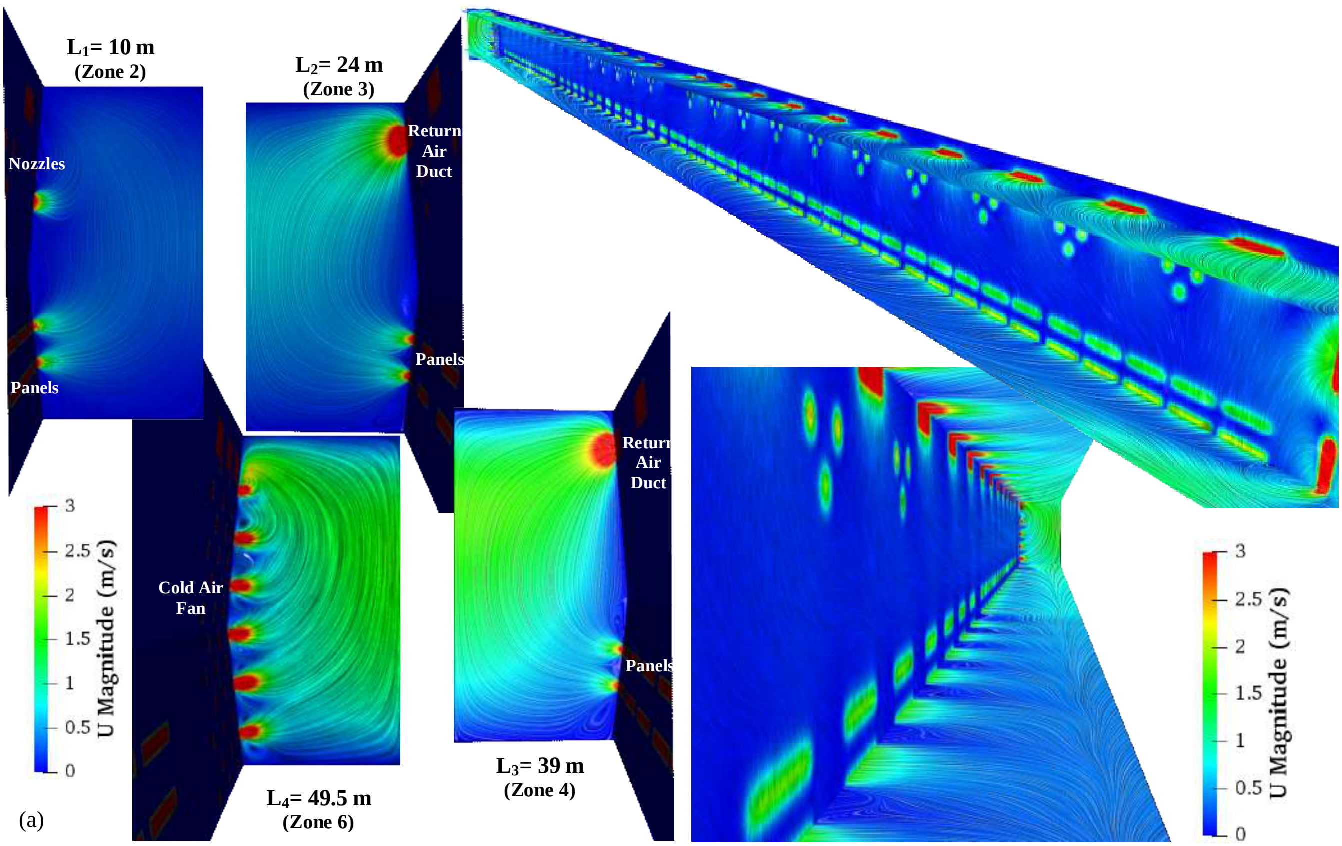

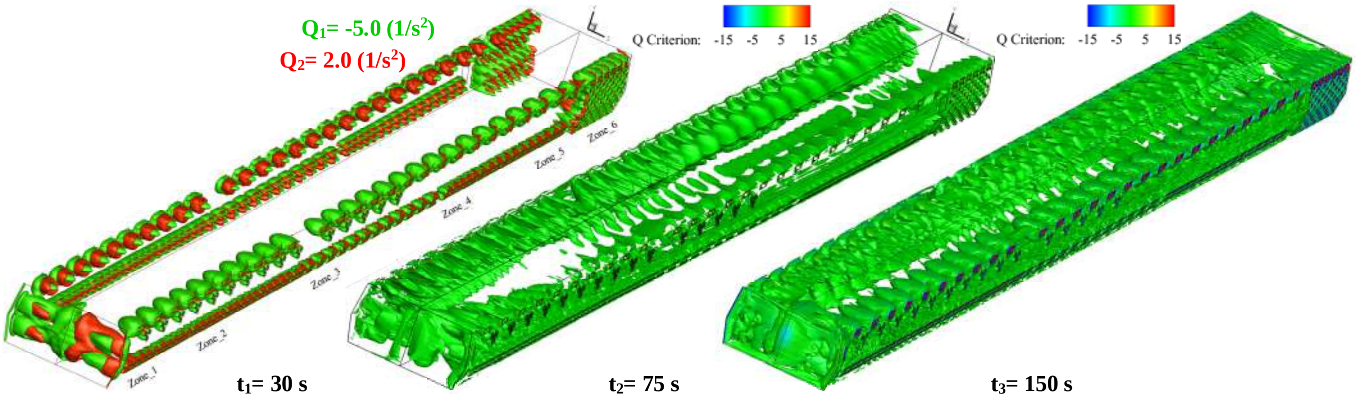

(b)

Fig. 27. (a) Evolution of vortical structures initial formation in critical planes using the LIC method (Stalling and Hege, 1997), with the velocity magnitude contour base (Oven_3, t= 150 s). (b) The three-dimensional iso-surfaces of the second invariant of the velocity gradient tensor Q (1/s^2) at the entire length of the oven volume (Oven_3 case): (a) t= 30 s, (b) t= 75 s, and (c) t= 150 s.

5. Concluding Remarks

The present study implements an optimization-based redesigning and parametric modification of conjugate heat transfer (CHT) in an entire automotive oven under the OpenFOAM framework as a reliable open-source tool. A precise fluid dynamic characteristic is obtained using an accurate LES turbulence model, high-fidelity solver, and high-quality structure grids after validating the proposed CHT code employing a heat sink benchmark. Notably, this is the first LES study revealing the impact of a whole automotive oven structural components on the heat and momentum transfer mechanisms over the car surface by fully resolving the process. Precise details for the base and modified ovens from the results of this unsteady simulation are compared – such as high-resolution flow distribution in different oven zones, diffusion pattern and mixing streams of various injected air streams, the convective heat transfer rate, vortical structures topology, velocity, and temperature fields map on the car body and inside the entire oven. The simulation results indicate that the implemented low-cost optimization strategy in the Oven_3 case, which involved manipulating the hot-air flow rate diffusion pattern, significantly intensified thermal energy efficiency during the CHT of the oven. The prominent air flow circulation happens at the middle and the end of the heat-up stage. This optimum thermal control guarantees the homogeneity and uniformity of the cured film with high quality in terms of visual appearance, corrosion, and durability. The present study further extends knowledge of curing mechanisms inside an automotive oven under heavy loading conditions.

Acknowledgements

This work was supported by Project "MOSIPO", project grant no. POCI-01-0247-FEDER-072621. The research was also partly supported by CMAST Center for Mechanical and Aerospace Science and Technology, research unit No. 151 (Project UID/00151/2020) from Fundacao para a Ciencia e Tecnologia (Portugal).

Reference

Agha, A. and Abu-Farha, F., 2021. Experimental methods to capture curing induced effects in adhesive bonded joints. International Journal of Adhesion and Adhesives, 104, p.102735.

Ajah, V. and Ejiogu, E., 2019. Solar Thermal/Electricity Paint Curing Oven. In 2019 IEEE International Conference on Sustainable Energy Technologies and Systems (ICSETS) (pp. 075-080). IEEE.

Albiez, C., Liewald, M., Görres, A. and Regensburger, J., 2011. Numerical prediction of thermal panel distortion incorporating thermal material properties of 6016 aluminum alloy. In Proceedings of European aluminium congress (pp. 11-23).

Ashrafizadeh, A., Mehdipour, R. and Rezvani, M., 2009, October. An efficient and accurate numerical simulation method for the paint curing process in auto industries. In ICADME Conference, Malaysia.

Bensow, R.E. and Fureby, C., 2007. On the justification and extension of mixed models in LES. Journal of Turbulence, (8), p.N54.

Bielski, S. and Malinowski, L., 2005. An analytical method for determining transient temperature field in a parallel-flow three-fluid heat exchanger. International Communications in Heat and Mass Transfer, 32(8), pp.1034-1044.

Brinckmann, F. and Stephan, P., 2011. Experimental investigation of the drying process of water-based paints used in automotive industry. Chemical Engineering and Processing: Process Intensification, 50(5-6), pp.489-494.

Cavalcante, E.S., Vasconcelos, L.G.S., de Farias Neto, G.W., Ramos, W.B. and Brito, R.P., 2020. Automotive painting process: Minimizing energy consumption by using adjusted convective heat transfer coefficients. Progress in Organic Coatings, 140, p.105479.

Chen, J.B., Sun, S.Q., Yu, J. and Zhou, Q., 2014. Tracking the curing process of automotive paint by moving-window two-dimensional infrared correlation spectroscopy and principal component analysis. Journal of Molecular Structure, 1069, pp.112-117.

Choi, J.W., Chun, W.P., Oh, S.H., Lee, K.J. and Kim, S.I., 2016. Experimental studies on a combined near infrared (NIR) curing system with a convective oven. Progress in Organic Coatings, 91, pp.39-49.

da Silva, V.A., de Neves Gomes, L.A.C., de Lima e Silva, A.L.F. and de Lima e Silva, S.M.M., 2019. Analysis of natural convection in heat sink using OpenFOAM and experimental tests. Heat and Mass Transfer, 55(8), pp.2289-2304.

De Villiers, E., 2006. The potential of large eddy simulation for the modeling of wall bounded flows. Imperial College of Science, Technology and Medicine.

Despotovic, M. and Babic, M., 2018. Analysis of different scenarios of car paint oven redesign to achieve desired indoor air temperature. Energy Efficiency, 11(4), pp.877-891.

Domnick, J., Gruseck, D., Pulli, K., Scheibe, A., Ye, Q. and Brinckmann, F., 2011. Investigations of the drying process of a water based paint film for automotive applications. Chemical Engineering and Processing: Process Intensification, 50(5-6), pp.495-502.

Ghosal, S., 1996. An analysis of numerical errors in large-eddy simulations of turbulence. Journal of Computational Physics, 125(1), pp.187-206.

Giampieri, A., Ling-Chin, J., Ma, Z., Smallbone, A. and Roskilly, A.P., 2020. A review of the current automotive manufacturing practice from an energy perspective. Applied Energy, 261, p.114074.

Harahap, F. and Rudianto, E., 2005. Measurements of steady-state heat dissipation from miniaturized horizontally-based straight rectangular fin arrays. Heat and mass transfer, 41(3), pp.280-288.

Issa, R.I., 1986. Solution of the implicitly discretised fluid flow equations by operator-splitting. Journal of computational physics, 62(1), pp.40-65.

Johnson, T., Mark, A., Sandgren, N., Erhardsson, L., Sandgren, S. and Edelvik, F., 2022. Efficient Simulation of Convective Ovens in Automotive Paintshops. Journal of Heat Transfer, 144(9), p.094501.

Kameš, J., 2014. Posouzení nového způsobu stříkání barvy.

Liu, F., 2016. A thorough description of how wall functions are implemented in OpenFOAM. Proceedings of CFD with OpenSource Software, 34.

Magnusson, J., 2010. Conjugate HeatFoam with explanational tutorial together with a buoyancy driven flow tutorial and a convective conductive tutorial. Magnusson's Technology Center, Chalmers University of Technology, Gothenburg.

Mishra, M., Das, P.K. and Sarangi, S., 2008. Dynamic behavior of three-fluid crossflow heat exchangers. Journal of heat transfer, 130(1).

Mulemane, A., Hurst, L., Fraser, A. and Sinclair, J., 2015. A reduced order model for simulating heat transfer processes in automotive paint shop ovens (No. 2015-01-0030). SAE Technical Paper.

Nazif, H.R., 2019. Improving the thermal efficiency of a car wax oven using CFD simulation and measurement. International Journal of Modelling and Simulation, 39(2), pp.125-134.

Niamsuwan, S., Kittisupakorn, P. and Suwatthikul, A., 2015. Enhancement of energy efficiency in a paint curing oven via CFD approach: Case study in an air-conditioning plant. Applied Energy, 156, pp.465-477.

Patankar, S.V. and Spalding, D.B., 1983. A calculation procedure for heat, mass and momentum transfer in three-dimensional parabolic flows. In Numerical Prediction of Flow, Heat Transfer, Turbulence and Combustion (pp. 54-73). Pergamon.

Pendar, M.R. and Páscoa, J.C., 2019. Numerical modeling of electrostatic spray painting transfer processes in rotary bell cup for automotive painting. International Journal of Heat and Fluid Flow, 80, p.108499.

Pendar, M.R. and Páscoa, J.C., 2022c. Numerical Investigation of Plasma Actuator Effects on Flow Control Over a Three-Dimensional Airfoil with a Sinusoidal Leading Edge. Journal of Fluids Engineering, 144(8), p.081208.

Pendar, M.R. and Roohi, E., 2018. Cavitation characteristics around a sphere: An LES investigation. International Journal of Multiphase Flow, 98, pp.1-23.

Pendar, M.R., Páscoa, J.C. and Lima, R., 2022b, August. Numerical investigation of automotive paint oven for improving the thermal efficiency. In Fluids Engineering Division Summer Meeting (Vol. 85840, p. V002T05A032). American Society of Mechanical Engineers.

Pendar, M.R., Rodrigues, F., Páscoa, J.C. and Lima, R., 2022a. Review of coating and curing processes: Evaluation in automotive industry. Physics of Fluids, 34(10), p.101301.

Prendi, L., Mills, M., Bastien, J. and Henshaw, P., 2015. Thermosetting powder coatings: Finish appearance and durability at cure window corner points. Progress in Organic Coatings, 78, pp.411-418.

Quarteroni, A. and Valli, A., 1999. Domain decomposition methods for partial differential equations (No. BOOK). Oxford University Press.

Rao, P. and Teeparthi, S., 2011, January. A semi–computational method to predict body temperatures in an automotive paint bake oven. In ASME International Mechanical Engineering Congress and Exposition (Vol. 54891, pp. 85-95).

Rao, P.P. and Gopinath, A., 2013. Energy savings in automotive paint ovens: a new concept of shroud on the carriers. Journal of Manufacturing Science and Engineering, 135(4).

Rao, P.P., 2013. A heat exchanger analogy of automotive paint ovens. Applied thermal engineering, 61(2), pp.381-392.

Roohi, E., Pendar, M.R. and Rahimi, A., 2016. Simulation of three-dimensional cavitation behind a disk using various turbulence and mass transfer models. Applied Mathematical Modelling, 40(1), pp.542-564.

Seubert, C.M. and Nichols, M.E., 2010. Epoxy thiol photolatent base clearcoats: curing and formulation. Journal of coatings technology and research, 7(5), pp.615-622.

Shrivastava, D. and Ameel, T.A., 2004. Three-fluid heat exchangers with three thermal communications. Part A: general mathematical model. International journal of heat and mass transfer, 47(17-18), pp.3855-3865.

Stalling, D. and Hege, H.-C., 1997. LIC on Surfaces. Texture Synthesis with Line Integral Convolution, pp. 51-64.

Stalling, D. and Hege, H.C., 1997. LIC on Surfaces. Texture Synthesis with Line Integral Convolution, pp.51-64.

Streitberger, H.J. and Dossel, K.F. eds., 2008. Automotive paints and coatings. John Wiley & Sons.

Sukhodolya, A., Cherepnina, T., Kostyuk, I. and Klimenko, V., 2021. Investigation of the paint curing mechanism. Transportation Research Procedia, 57, pp.667-671.

Vasudevan, M., 2018. Numerical modelling of paint curing in convective ovens (Master's thesis).

Wonnemann, H., 2008. Primer surfacer. Automotive Paints and Coatings, pp.129-174.

Wu, Y.H., Srinivasan, K., Patterson, S. and Bot, E., 2013, July. Transient thermal analysis for the automotive underhood and underbody components. In Heat Transfer Summer Conference (Vol. 55508, p. V004T14A028). American Society of Mechanical Engineers.

Xiao, J., Li, J., Lou, H.H. and Huang, Y., 2006. Cure-window-based proactive quality control in topcoat curing. Industrial & engineering chemistry research, 45(7), pp.2351-2360.

Ye, Q., Pulli, K., Scheibe, A., Domnick, J. and Gruseck, D., 2009, July. Numerical simulation of turbulent heat transfer in industrial drying processes. In Proceeding of the 4th EASC 2009, European Automotive Simulation Conference.

Yu, G., 2013. Simulation of automotive paint curing process in an oven. Metal finishing, 2(111), pp.18-22.

Zelder, G. and Steinbeck-Behrens, C., 2009. Simulation on Car Body Painting Processes. no. July, pp.2-7.

Highlights

- Proposal of a comprehensive methodology for numerical evaluation of an automotive multi-zone oven's drying/curing process.
- Development of an efficient conjugate heat transfer (CHT) algorithm under the OpenFOAM package framework.
- Implementation of an optimization-based redesigning and effective parametric modification of conjugate heat transfer in an automotive oven with car chassis.
- Providing a thorough analysis of the fluid dynamic characteristics, e.g., thermal diffusion pattern, vortical structure/nature, and temperature fields map across all the modified oven.
- Obtaining the optimum thermal control and energy efficiency guarantees the high-quality cured film's homogeneity.

Declaration of interests

☒The authors declare that they have no known competing financial interests or personal relationships that could have appeared to influence the work reported in this paper.

☐The authors declare the following financial interests/personal relationships which may be considered as potential competing interests: